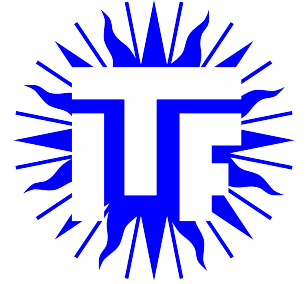




Universiteit Utrecht



Faculteit Bètawetenschappen

# Steady State of an Ideal Active Lattice Gas: Accumulation at Boundaries and Ratchet Potentials

BACHELOR THESIS

*Marjolein de Jager*

Natuur- en Sterrenkunde

*Supervisors:*

Prof. RENÉ VAN ROIJ  
Institute for Theoretical Physics

JEROEN RODENBURG MSc.  
Institute for Theoretical Physics

January 2017

## Abstract

This thesis examines the steady states of ideal active Brownian particles on a discrete lattice and aims to find the generalisation of the Boltzmann distribution for active systems. We specifically study the dependence on the particle activity of the particle accumulation at hard wall boundaries and the influence of an external ratchet potential on the steady state. We develop a model that describes the system in terms of discrete probabilities for particles to move from position and orientation  $(\vec{r}, \hat{e})$  at time  $t$  to  $(\vec{r}', \hat{e}')$  at time  $t + \tau$ . We find that the magnitude of the particle accumulation at the boundaries is proportional to the Péclet number  $Pe$  squared and that it decays with a universal decay length proportional to  $1/\sqrt{1 + Pe^2}$ . The presence of an external ratchet potential causes the steady state to divide into two subsystems with their own bulk densities. The bulk density is highest at the steepest side of the ratchet and we numerically determine the dependency of the difference in bulk densities on the Péclet number for the high and low  $Pe$  regime and on the height, length and asymmetry of the ratchet for flat, long and almost symmetric ratchet potentials.

## Contents

<b>1</b>	<b>Introduction</b>	<b>1</b>
1.1	Brownian Motion . . . . .	1
1.2	Active Brownian Motion . . . . .	2
<b>2</b>	<b>One-Parameter Model</b>	<b>4</b>
2.1	Time Evolution of a State . . . . .	4
2.2	The Steady State . . . . .	5
2.3	Two-Dimensional System . . . . .	6
<b>3</b>	<b>Two-Parameter Model</b>	<b>7</b>
3.1	Time Evolution and Steady State . . . . .	7
3.2	Rotation of Particle Flux . . . . .	9
3.3	Continuum Limit and Analogy with Continuous Model . . . . .	10
3.4	One-Dimensional Solutions of the Fokker-Planck Equation . . . . .	12
3.5	Wall Pressure . . . . .	14
3.6	Comparison with Continuum Model . . . . .	14
<b>4</b>	<b>Two-Parameter Model with Ratchet Potential</b>	<b>16</b>
4.1	Ratchet Force and Time Evolution of a State . . . . .	16
4.2	Examples of Steady States . . . . .	17
4.3	Bulk Density Difference . . . . .	19
<b>5</b>	<b>Conclusion, Discussion and Outlook</b>	<b>22</b>
5.1	Conclusion . . . . .	22
5.2	Discussion . . . . .	22
5.3	Outlook . . . . .	23
<b>6</b>	<b>Acknowledgement</b>	<b>24</b>
<b>A</b>	<b>Eigenvalues of the Transition Matrix</b>	<b>25</b>
<b>B</b>	<b>Continuum Limit of Lattice Model with Ratchet Potential</b>	<b>26</b>
	<b>References</b>	<b>II</b>

# 1 Introduction

In recent years there has been a strong growth in both theoretical and experimental research regarding *active matter*. A system is called “active” when its particles have the ability to move on their own due to a self-propulsion mechanism. Countless examples of active systems appear in nature, such as microswimmers, including bacteria [1–3], water fleas [4], and algae [5], flocks of birds and butterflies or schools of fish [6–9]. Studies on synthetically prepared self-propelled colloids, e.g. colloidal particles propelled through phoretic forces [10, 11] or laser-heated metal-capped particles [12], have revealed intriguing phenomena arising in active systems, including accumulation at boundaries [13–15], clustering [11], spontaneous self-induced flow [16, 17] and long-range depletion-induced forces [18].

Unlike active systems, passive systems have been studied for almost two centuries and perform a well known phenomenon: *Brownian motion*, which is the random motion of particles suspended in a fluid [19]. A thoroughly studied subject considering passive systems is the effect of an external potential. It has been shown that, in presence of an external potential  $V(\vec{r})$ , the probability distribution of a passive system in equilibrium is given by the Boltzmann distribution

$$P_0(\vec{r}) = \mathcal{N}e^{-\beta V(\vec{r})}, \quad (1.1)$$

where  $\mathcal{N}$  is a proper normalisation factor, such that  $\int d\vec{r}P_0(\vec{r}) = 1$  [20].

This thesis addresses the key question: “*What is the generalisation of the Boltzmann distribution for active systems?*”. We specifically study the particle accumulation at hard wall boundaries and the density difference at either side of an external ratchet potential.

## 1.1 Brownian Motion

In 1827 botanist Robert Brown discovered the phenomenon that is nowadays called *Brownian motion* [19]. At first Brown ascribed the observed never-vanishing random motion of small pollen of grain immersed in a liquid to living entities. However, repeating the experiments using glass granules he observed the same non-vanishing erratic motion. A couple of decades later the origin of Brownian motion was traced back to the motion of the surrounding liquid molecules colliding with the particles [21] and early twentieth century great minds like Albert Einstein [22], Paul Langevin [23], Marian von Smoluchowski [24], and others theoretically proved this origin. In the decades that followed Brownian motion played a key role in the foundation of thermodynamics and statistical physics and it still serves as a rich source of research today.

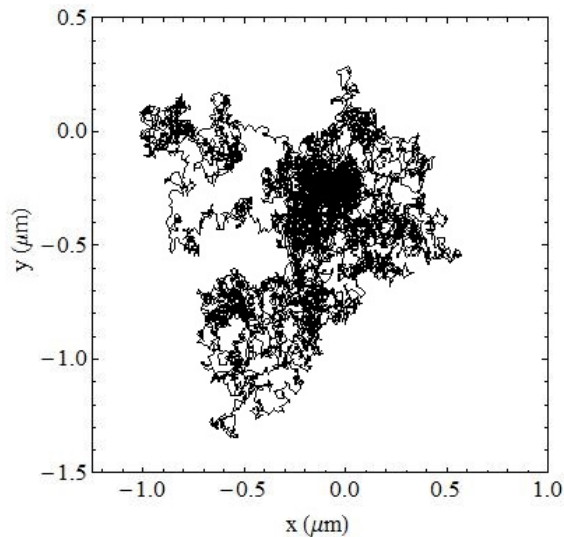


Figure 1: Two-dimensional trajectory of a Brownian particle with translational diffusion coefficient  $D_t = 0.16\mu\text{m}^2/\text{s}$ . The particle started from the origin and the figure shows the trajectory during 30s. Figure is taken from <http://physicsweb.phy.uic.edu/450/MARK0/N004.html> at December 8, 2017.

A Brownian particle immersed in a fluid is constantly moving in always randomly changing directions due to collisions with the surrounding molecules of the medium. A two-dimensional trajectory of a Brownian particle is shown in figure 1. The particle started from the origin and its trajectory clearly displays the random nature of Brownian motion. The Newtonian dynamics of a single Brownian sphere with mass  $m$ , radius  $R$ , position  $\vec{r}$  and velocity  $\vec{v}$  are governed by the Langevin equation

$$\frac{d\vec{r}}{dt} = \vec{v}, \quad m \frac{d\vec{v}}{dt} = -\gamma\vec{v} - \nabla V(\vec{r}) + \vec{F}(t), \quad (1.2)$$

where  $\gamma = 6\pi\eta R$  is the friction coefficient given by Stokes law,  $\eta$  the viscosity of the solvent,  $V(\vec{r})$  a space-dependent potential, and  $\vec{F}(t)$  a short correlated stochastic force, which describes the effect of the background noise due to fluid particles [25]. Ornstein and Uhlenbeck showed that  $\vec{F}(t)$  should be a Gaussian white noise, such that

$$\vec{F}(t) = \gamma\sqrt{2D_t}\vec{\xi}(t), \quad \langle \vec{\xi}(t) \rangle = 0, \quad \langle \xi_i(t)\xi_j(t') \rangle = \delta_{i,j}\delta(t-t'), \quad i, j = x, y, z, \quad (1.3)$$

where  $\langle \vec{\xi}(t) \rangle$  is the expectation value of the random noise vector  $\vec{\xi}(t)$  and  $D_t$  the translational diffusion coefficient of the Brownian particle given by the fluctuation-dissipation theorem derived by Einstein [20]

$$D_t = \frac{k_B T}{\gamma}, \quad (1.4)$$

with  $k_B$  the Boltzmann constant and  $T$  the absolute temperature of the fluid.

Many systems often show overdamped Brownian motion, where  $m \frac{d\vec{v}}{dt} = 0$ , on observable time scales. Bacteria and other microswimmers, for example, usually perform overdamped Brownian motion dominated by friction. The Langevin equation in the overdamped limit reads

$$\frac{d\vec{r}}{dt} = \vec{v} = -\beta D_t \nabla V(\vec{r}) + \sqrt{2D_t}\vec{\xi}(t), \quad (1.5)$$

where  $\beta = 1/k_B T$ . Using a probabilistic description, all the information of a system is captured by the probability  $P(\vec{r}, t | \vec{r}_0, t_0)$  to find a particle at location  $\vec{r}$  at time  $t$  if it started at  $\vec{r}_0$  at  $t_0$ . The overdamped Fokker-Planck equation, which describes a particle satisfying the equation of motion Eq.(1.5), is given by

$$\frac{\partial P(\vec{r}, t | \vec{r}_0, t_0)}{\partial t} = \beta D_t \frac{\partial}{\partial \vec{r}} [\nabla V(\vec{r}) P] + D_t \frac{\partial^2 P}{\partial \vec{r}^2}. \quad (1.6)$$

The density distribution which corresponds to the long-time limit solution of Eq.(1.5) is the steady state solution, where  $\frac{\partial P(\vec{r}, t | \vec{r}_0, t_0)}{\partial t} = 0$ . The steady state solution is independent of the starting position and times  $t_0$  and  $t$  and is given by the Boltzmann distribution

$$P(\vec{r}, t | \vec{r}_0, t_0) = P_0(\vec{r}) = \mathcal{N} e^{-\beta V(\vec{r})}, \quad (1.7)$$

where  $\mathcal{N}$  is a proper normalisation factor, such that  $\int d\vec{r} P_0(\vec{r}) = 1$  [20].

## 1.2 Active Brownian Motion

Active Brownian particles, or ABPs in short, have the capability to extract energy from their environment and convert it into systematic movement. Apart from motion due to collisions with the surrounding fluid molecules, ABPs also undergo motion due to its environmentally fuelled self-propulsion force. The motion of ABPs is no longer a random motion: it is “biased”, which means that a particle is more likely to travel along the direction of its self-propulsion force than along any other direction. The orientation of an ABP is the direction of the self-propulsion. It is often set by the structure of the particle, e.g. particles can be elongated along their direction of self-propulsion or the direction can depend on the placement of the metal cap, rather than being fixed by an external factor. Orientational order of active systems is a heavily researched topic [26, 27].

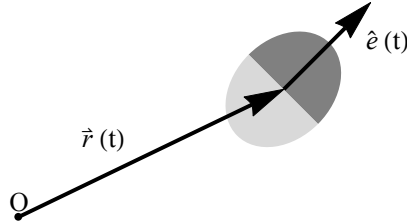


Figure 2: Schematic visualisation of an active Brownian particle with position  $\vec{r}(t)$  and orientation  $\hat{e}(t)$ .

The dynamics of an ABP are given by its time-dependent position  $\vec{r}(t)$  and orientation  $\hat{e}(t)$  and are governed by the Langevin equation. Here  $\hat{e}(t)$  is a unit vector. A schematic visualisation of an ABP is shown in figure 2. For an overdamped ABP the Langevin equations reads

$$\frac{d\vec{r}}{dt} = -\beta D_t \nabla V(\vec{r}) + v_0 \hat{e} + \sqrt{2D_t} \vec{\xi}_t(t), \quad \frac{d\hat{e}}{dt} = \sqrt{2D_r} \vec{\xi}_r(t), \quad (1.8)$$

where  $v_0$  is the self-propulsion speed,  $D_t$  and  $D_r$  are the translation and rotation diffusion coefficients, and  $\vec{\xi}_t(t)$  and  $\vec{\xi}_r(t)$  are the translation and rotation Gaussian white noises that satisfy  $\langle \vec{\xi}_t(t) \rangle = \langle \vec{\xi}_r(t) \rangle = 0$  and  $\langle \xi_{t,i}(t) \xi_{t,j}(t') \rangle = \langle \xi_{r,i}(t) \xi_{r,j}(t') \rangle = \delta_{i,j} \delta(t - t')$  for  $i, j = x, y, z$ . The overdamped Fokker-Planck equation is now given by [28]

$$\frac{\partial P(\vec{r}, \hat{e}, t | \vec{r}_0, \hat{e}_0, t_0)}{\partial t} = \frac{\partial}{\partial \vec{r}} [\beta D_t \nabla V(\vec{r}) - v_0 \hat{e}] P + D_t \frac{\partial^2 P}{\partial \vec{r}^2} + D_r \frac{\partial^2 P}{\partial \hat{e}^2}. \quad (1.9)$$

In this thesis we develop a model to describe ideal active Brownian particles on a discrete lattice of position  $\vec{r}$  and orientation  $\hat{e}$  and discrete times  $t$ . For such a discrete case, the system can be described in terms of discrete probabilities that a particle moves from  $i = (\vec{r}, \hat{e})$  at time  $t$  to  $j = (\vec{r}', \hat{e}')$  at time  $t + \tau$ , which is in fact described by a matrix with entries  $M_{ji}$ . We will see that the time evolution of the system is governed by eigenvalues and eigenvectors of the transition matrix  $M$  and use this to determine the steady state of the system characterised by  $\frac{\partial P}{\partial t} = 0$ . The big advantage of our discrete model over a continuum model or simulations is the simplicity and intuitiveness with which our model is described and its short calculation time.

In the first half of this thesis we develop the model for a one-dimensional lattice with hard wall boundary conditions and no other external potential and compare our results of the steady state with a continuum calculation. In the second half we implement an external ratchet potential and analyse its effect on the steady state.

## 2 One-Parameter Model

In this chapter we look at an extremely simplified model for an active lattice gas in a system with no external potential. We shall see that this model is too heavily simplified to produce all the characteristics of a continuum active system and therefore suggest a modified model in the next chapter. The approach for both models, however, is identical. First, we look at the description of the model for a one-dimensional lattice and later at a two-dimensional lattice.

Consider an ideal gas on a one-dimensional lattice of length  $L = (N - 1)a$ , where  $N$  is the number of sites and  $a$  the lattice constant. We use hard wall boundary conditions, such that particles cannot escape out of the lattice. A particle on site  $i = 1, \dots, N$  can have an orientation to the right, i.e.  $e_i = +1$ , or to the left,  $e_i = -1$ . The particle probability distribution at time  $t$  is described by the state vector

$$|n(t)\rangle = (n_{1,-}(t), n_{1,+}(t), \dots, n_{i,-}(t), n_{i,+}(t), \dots, n_{N,-}(t), n_{N,+}(t))^T, \quad (2.1)$$

where  $n_{i,-}(t)$  and  $n_{i,+}(t)$  are the number of particles at site  $i$  at time  $t$  with orientation  $e = -1$  and  $e = +1$ , respectively, for  $i = 1, \dots, N$ . As we consider non-interacting lattice gasses, there can be multiple particles on a lattice site. The state vector has length  $2N$ .

### 2.1 Time Evolution of a State

The time evolution of  $|n(t)\rangle$  can be described by two consecutive processes: rotation and translation. During one time step  $\tau$  the new orientations of the particles are determined in the rotation step first, before the particles propagate along their orientation in the translation step. A particle's orientation can either be maintained or changed during the rotation step. A change in the orientation is caused by collisions with the fluid particles. For passive matter the orientation after a sufficiently long time step should be random and independent of the previous orientation in order to reproduce Brownian motion. As a result, the probabilities of maintaining or changing the orientation should be equal for passive matter. For active matter, however, the probability of maintaining its orientation should be greater than the probability of changing it. To provide a measure for the activity of system we introduce the parameter  $\gamma \in [0, \frac{1}{2}]$ , where  $\gamma = \frac{1}{2}$  indicates passive matter and  $\gamma = 0$  perfectly active matter. A particle with pre-rotational state  $n_{i,e}(t)$  has post-rotational state  $n'_{i,e}(t)$  with probability  $1 - \gamma$  or  $n'_{i,-e}(t)$  with probability  $\gamma$ . We can capture the rotations of the particle orientation at site  $i$  with the  $2 \times 2$  matrix equation

$$\begin{pmatrix} n'_{i,-}(t) \\ n'_{i,+}(t) \end{pmatrix} = \underbrace{\begin{pmatrix} 1 - \gamma & \gamma \\ \gamma & 1 - \gamma \end{pmatrix}}_{m_R} \begin{pmatrix} n_{i,-}(t) \\ n_{i,+}(t) \end{pmatrix}. \quad (2.2)$$

Using this equation we can construct the rotation matrix  $R$  for the state vector, which obeys

$$|n'(t)\rangle = R|n(t)\rangle, \quad (2.3)$$

where  $R$  is a  $2N \times 2N$  block diagonal matrix with the  $2 \times 2$  matrix  $m_R$  on its diagonal.

Directly after the rotation step the particles translate along their orientation. For particles at site  $i \neq 1, N$  this is captured in the following translation equations

$$n_{i,-}(t + \tau) = n'_{i+1,-}(t), \quad (2.4)$$

$$n_{i,+}(t + \tau) = n'_{i-1,+}(t). \quad (2.5)$$

For particles at sites  $i = 1$  and  $i = N$  we need to implement our hard wall boundary conditions. The presence of a wall has two consequences: (i) particles cannot propagate through the wall and (ii) particles that collide with the wall will maintain their position and orientation. These consequences result in the following equations for particles at the left ( $i = 1$ ) and right wall ( $i = N$ )

$$n_{1,-}(t + \tau) = n'_{2,-}(t) + n'_{1,-}(t), \quad (2.6)$$

$$n_{1,+}(t + \tau) = 0, \quad (2.7)$$

$$n_{N,-}(t + \tau) = 0, \quad (2.8)$$

$$n_{N,+}(t + \tau) = n'_{N-1,+}(t) + n'_{N,+}(t). \quad (2.9)$$

Using Eq.(2.4)-(2.9) we can construct a translation matrix  $T'$  for the state vector, which obeys

$$|n(t + \tau)\rangle = T'|n'(t)\rangle, \quad (2.10)$$

with  $T'$  a  $2N \times 2N$  block matrix constructed using two  $2 \times 2$  matrices  $m_1$  and  $m_2$ :

$$m_1 = \begin{pmatrix} 1 & 0 \\ 0 & 0 \end{pmatrix}, \quad m_2 = \begin{pmatrix} 0 & 0 \\ 0 & 1 \end{pmatrix}, \quad T' = \begin{pmatrix} m_1 & m_1 & & & \\ m_2 & 0 & m_1 & & \\ & \ddots & \ddots & \ddots & \\ & & m_2 & 0 & m_1 \\ & & & m_2 & m_2 \end{pmatrix}. \quad (2.11)$$

Now, by combining Eq.2.3) and Eq.(2.10) we get our final matrix equation for the time evolution of the state vector

$$|n(t)\rangle = M'|n(t - \tau)\rangle = (M')^{t/\tau} |n(0)\rangle, \quad (2.12)$$

where  $M' = T'R$  is the  $2N \times 2N$  transition matrix,  $|n(0)\rangle$  the initial state, and  $t/\tau$  an integer.

## 2.2 The Steady State

In the previous section we arrived at a matrix equation for the time evolution of a state (Eq.(2.12)). The transition matrix  $M'$  in this equation contains all the information of our model. In the limit of  $t \rightarrow \infty$  the system reaches its steady state. For a system that has reached its steady state the following identity holds:  $|n(t + \tau)\rangle = |n(t)\rangle$ . Thus, to find the steady state  $|n_{ss}\rangle$  we simply have to solve

$$(M' - \mathbb{1}) |n_{ss}\rangle = 0. \quad (2.13)$$

This corresponds to finding the eigenvector of  $M'$  belonging to the eigenvalue  $\mu = 1$ . When  $\gamma \neq 0$ ,  $\mu$  is unique. Yet, in the extreme case where  $\gamma = 0$ ,  $M'$  has two eigenvalues that are equal to 1.<sup>1</sup> This, however, does not affect the calculation of the steady state, it only results in two possible steady states.

We use *Mathematica* to analytically find the steady state. As can be seen shortly the system has a bulk and we rescale the steady state such that the density of the bulk is equal to 1. The steady state vector is of the form

$$|n_{ss}\rangle = \left( \frac{1}{2\gamma}, 0, \frac{1}{2}, \frac{1}{2}, \frac{1}{2}, \frac{1}{2}, \dots, \frac{1}{2}, \frac{1}{2}, \frac{1}{2}, \frac{1}{2}, 0, \frac{1}{2\gamma} \right)^T, \quad (2.14)$$

and apart from the fact that it has length  $2N$ , the form is independent of  $N$ . Given a certain state vector, the particle density  $\rho_i$  and polarisation  $m_i$  on site  $i$  are defined by

$$\rho_i = n_{i,+} + n_{i,-}, \quad m_i = n_{i,+} - n_{i,-}. \quad (2.15)$$

Using this and Eq.2.14 we calculate the steady state density and polarisation vectors of length  $N$ . They are given by

$$|\rho_{ss}\rangle = \left( \frac{1}{2\gamma}, 1, 1, \dots, 1, 1, \frac{1}{2\gamma} \right)^T, \quad |m_{ss}\rangle = \left( \frac{-1}{2\gamma}, 0, 0, \dots, 0, 0, \frac{1}{2\gamma} \right)^T. \quad (2.16)$$

We see that the density is homogeneously distributed for passive matter ( $\gamma = \frac{1}{2}$ ), as is expected of a system with ideal Brownian particles and no external potential. For active matter ( $0 \leq \gamma < \frac{1}{2}$ ), however, we get an accumulation of particles at the walls. We also see that the net polarisation of the particles is negative at the left wall and positive at the right wall, thus the particles have an orientation which points towards the wall directly next to them. This is explained by the fact that particles, which collide with the wall, keep their position and orientation. Since an active particle has a larger probability of keeping its orientation than of changing it, a particle, once it collides with the wall, tends to “get stuck” at the wall. Notice that  $n_{i,+1} = n_{N,-1} = 0$  in Eq.(2.14). This means that there can be no particles at the site directly next to a wall with an orientation away from the wall. Consequently, the polarisation at the sites  $i = 1$  and  $i = N$  is always non-zero, even when we consider passive particles. This is due to the fact that we look at states after the

<sup>1</sup>See appendix A for a study on the transition matrix and its eigenvalues.



translation step. Once a particle at site  $i = 1$  or  $i = N$  changes its orientation during the orientation step, such that it points away from the wall, the particle will immediately translate to site 2 or  $N - 1$  during the translation step.

Furthermore, notice that the accumulation and polarisation at the wall do not extend into the bulk any further than the site directly in contact with the wall, i.e. there is no length scale in the system other than the lattice spacing  $a$ . This lack of additional length scale is the most obvious indication for the oversimplification of this model, since experiments with and continuum models of active matter systems do show one or more length scales [13–15, 18].

### 2.3 Two-Dimensional System

Although we already saw in the previous section that the model of this chapter is oversimplified, we will briefly look at its two-dimensional version in this section. Using the same method as for the one-dimensional lattice, we start by defining the state vector for a gas on a two-dimensional lattice of  $N_L \times N_B$  sites. For the state to be represented by a vector we do not label the lattice sites using coordinates, but simply count the sites one row after the other. The sites of a  $3 \times 3$  lattice, for example, are counted as follows

1	2	3
4	5	6
7	8	9

Now, using that the orientation of a particle can either be up, down, right or left, we get the state vector

$$|n^{2D}(t)\rangle = (n_{1,u}(t), n_{1,d}(t), n_{1,r}(t), n_{1,l}(t), \dots, n_{N_L N_B, u}(t), n_{N_L N_B, d}(t), n_{N_L N_B, r}(t), n_{N_L N_B, l}(t))^T, \quad (2.17)$$

where  $n_{i,u}(t)$ ,  $n_{i,d}(t)$ ,  $n_{i,r}(t)$  and  $n_{i,l}(t)$  are the number of particles at site  $i = 1, \dots, N_L N_B$  at time  $t$  with orientation up, down, right and left, respectively. The state vector has length  $4N_L N_B$ .

Following the same steps as in section 2.1, it is quite straightforward to construct a matrix analogous to  $M'$  for a two-dimensional active lattice gas. Similarly to the one-dimensional case we find the steady state using Eq.(2.13). The steady state shows only accumulation and net polarisation at the sites directly next to the walls, with a larger accumulation and net polarisation at the corner sites. Again we find a system without a length scale. The exact densities and polarisations for a square lattice are independent of  $N_L = N_B = N$  for  $N \geq 3$  and are given by Eq.(2.18). A representation of the density and polarisation distribution of a  $5 \times 5$  lattice is shown in figure 3. Notice that, like in the one-dimensional case, the density distribution is homogeneous for passive systems ( $\gamma = \frac{1}{2}$ ) and the polarisation at the walls is always non-zero.

$$\rho = \begin{cases} 1 & \text{bulk,} \\ \frac{1}{2\gamma} & \text{wall,} \\ \frac{1}{4\gamma^2} & \text{corner,} \end{cases} \quad |\vec{m}| = \begin{cases} 0 & \text{bulk,} \\ \frac{1}{4\gamma} & \text{wall,} \\ \frac{1}{4\sqrt{2}\gamma^2} & \text{corner.} \end{cases} \quad (2.18)$$

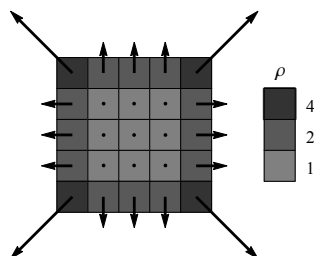


Figure 3: Steady state of active ideal gas on a  $5 \times 5$  lattice for  $\gamma = \frac{1}{4}$ . The arrows represent the polarisation and the darkness of a site is a measure for the density.

### 3 Two-Parameter Model

As already mentioned in the previous chapter, the one-parameter model is oversimplified which results in an absence of length scales other than the lattice spacing in both the one- and two-dimensional system. This absence of an additional length scale has its origin in the translation step of the time evolution. In the previous chapter we assumed that, once the orientation of a particle is determined in the rotation step, a particle will always propagate along this orientation in the translation step. However, we omitted the ability of fluid particles to not only change the orientations of ABPs, but also to force them to translate in a different direction than their orientation. The importance of this process with respect to the self-propulsion depends on the activity of the matter. In this chapter, we first modify the lattice model such that it also takes the influence of fluid particles during the translation step into account and we then compare it to a continuum model of ABPs.

#### 3.1 Time Evolution and Steady State

For our two-parameter model we can largely use the one-parameter model described in chapter 2, since we only treat the translation step differently. We therefore use the state vector described by Eq.(2.1) and the rotation matrix described by Eq.(2.2). For the translation matrix we introduce the parameter  $\alpha$ , which is a measure for the importance of self-propulsion relative to that of Brownian motion. For  $\alpha = 0$  we have passive matter. The Brownian motion should completely dominate the self-propulsion for passive matter, thus the probability to propagate in any direction should be equal for all directions. When  $\alpha > 0$  the self-propulsion starts to play a role and as a result the probability of a particle propagating along its orientation exceeds the probability to propagate in any other direction. Recall that for a one-dimensional lattice there are only two directions.

Keeping this in mind, we construct the following translation equations for particles on site  $i \neq 1, N$

$$n_{i,-}(t + \tau) = \frac{1 + \alpha}{2} n'_{i+1,-}(t) + \frac{1 - \alpha}{2} n'_{i-1,-}(t), \quad (3.1)$$

$$n_{i,+}(t + \tau) = \frac{1 + \alpha}{2} n'_{i-1,+}(t) + \frac{1 - \alpha}{2} n'_{i+1,+}(t), \quad (3.2)$$

where  $\frac{1+\alpha}{2}$  is the probability to translate along its orientation and  $\frac{1-\alpha}{2}$  the probability to translate in the opposite direction. It is important to note that particles are not allowed to change their orientation during the translation step. Further note that we get the translation equations from chapter 2 for  $\alpha = 1$ .

Particles at sites  $i = 1, N$  experience the same consequences due to the hard wall boundary conditions as described in section 2.1, i.e. there is no flux in or out of the wall and particles that collide with the wall maintain their position and orientation. Taking these consequences into account we get the following translation equations for particles at the walls

$$n_{1,-}(t + \tau) = \frac{1 + \alpha}{2} n'_{2,-}(t) + \frac{1 + \alpha}{2} n'_{1,-}(t), \quad (3.3)$$

$$n_{1,+}(t + \tau) = \frac{1 - \alpha}{2} n'_{2,+}(t) + \frac{1 - \alpha}{2} n'_{1,+}(t), \quad (3.4)$$

$$n_{N,-}(t + \tau) = \frac{1 - \alpha}{2} n'_{N-1,-}(t) + \frac{1 - \alpha}{2} n'_{N,-}(t), \quad (3.5)$$

$$n_{N,+}(t + \tau) = \frac{1 + \alpha}{2} n'_{N-1,+}(t) + \frac{1 + \alpha}{2} n'_{N,+}(t). \quad (3.6)$$

Eq.(3.1)-(3.6) can be written in terms of the  $2N \times 2N$  translation matrix equation

$$|n(t + \tau)\rangle = T|n'(t)\rangle, \quad (3.7)$$

with  $T$  the  $2N \times 2N$  block matrix constructed using the  $2 \times 2$  matrices  $m_{\pm}$ :

$$m_{\pm} = \begin{pmatrix} \frac{1 \pm \alpha}{2} & 0 \\ 0 & \frac{1 \mp \alpha}{2} \end{pmatrix}, \quad T = \begin{pmatrix} m_+ & m_+ & & & & \\ m_- & 0 & m_+ & & & \\ & \ddots & \ddots & \ddots & & \\ & & m_- & 0 & m_+ & \\ & & & m_- & m_- \end{pmatrix}. \quad (3.8)$$

Having defined the translation matrix, the transition matrix for our two-parameter model is given by  $M = TR$ . The steady state of the system is, once again, found by calculating the eigenvector belonging to the unique eigenvalue  $\mu = 1$ .<sup>2</sup> Unfortunately, *Mathematica* is not able to find an analytical solution for the steady state of this model for arbitrary  $N$ . A numerical solution, however, can be found straightforwardly using *Mathematica* for fixed finite  $N$ .

Figure 4a and 4b show the density and polarisation distribution of the steady state for  $(\alpha, \gamma)$  combinations given by  $(0.01, 0.001)$ ,  $(0.01, 0.002)$ ,  $(0.02, 0.01)$  and  $(0.02, 0.005)$ . These results were obtained using a lattice of  $N = 251$  sites and scaling the calculated steady states such that the density at the middlemost site ( $i = 126$ ), i.e. the bulk density, is equal to 1. In contrast to our one-parameter model, this two-parameter model clearly shows a length scale in the accumulation at the wall. A logarithmic plot, see figure 4c, reveals an exponential decay of the density and polarisation distribution at the wall. More precisely, the density and polarisation at the left wall are given by

$$\rho(x) = \rho_{\text{bulk}} + \rho_{\text{wall}} e^{-x/\lambda_\rho}, \quad (3.9)$$

$$m(x) = -m_{\text{wall}} e^{-x/\lambda_m}, \quad (3.10)$$

with  $x$  the distance from the wall,  $\rho_{\text{bulk}}$  the density of the bulk,  $\rho_{\text{wall}}$  and  $m_{\text{wall}}$  the density and absolute polarisation directly at the wall, and  $\lambda_\rho$  and  $\lambda_m$  the decay length of the density and polarisation.

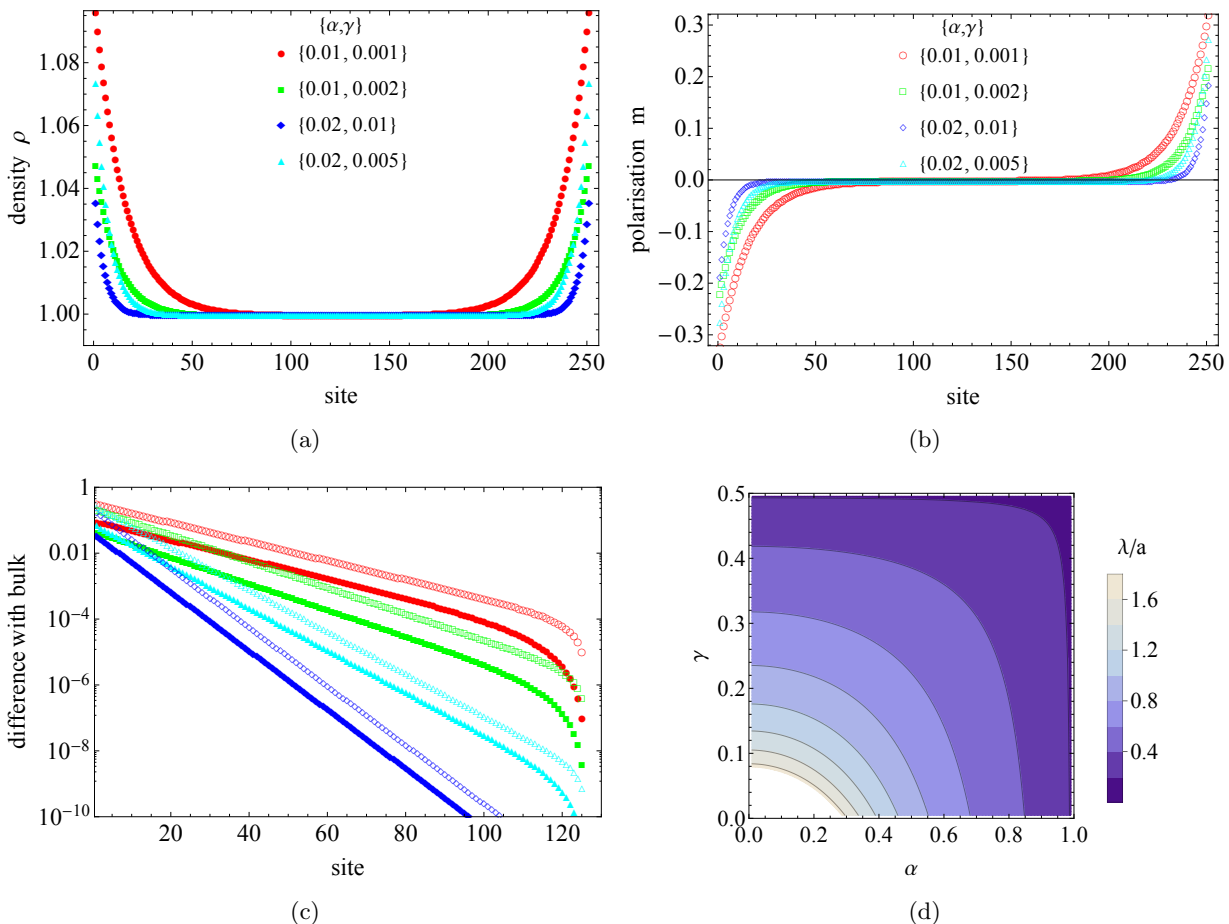


Figure 4: Density (a) and polarisation (b) of the steady state for selected model parameters  $\alpha$  and  $\gamma$  (see text). (c) Logarithmic plot of the difference between the site and bulk density or polarisation revealing an exponential decay with characteristic decay length  $\lambda$ , which is equal for the density and polarisation of each system. (d) Contour plot of the decay length  $\lambda$  scaled by the lattice constant  $a$  versus  $\alpha$  and  $\gamma$ .

<sup>2</sup>See appendix A for a study on the transition matrix and its eigenvalues.

Notice that the density and polarisation belonging to a certain  $\alpha$  and  $\gamma$  seem to have equal slopes in the logarithmic plot of figure 4c, this indicates equal decay lengths. To find the decay lengths  $\lambda_\rho$  and  $\lambda_m$  we fit our results to Eq.(3.9) and Eq.(3.10). We indeed find  $\lambda_\rho = \lambda_m = \lambda$  within a relative numeric precision of  $10^{-10}$ . Figure 4d shows a contour plot of the scaled decay length  $\frac{\lambda}{a}$  versus  $\alpha$  and  $\gamma$ . To construct this contour plot we calculated  $\lambda$  for a lattice of  $N = 251$  sites with  $\alpha$  and  $\gamma$  taken over their total range in steps of 0.01 and 0.005, respectively. We see that  $\lambda$  is large for small  $\alpha$  and  $\gamma$  and small for large  $\alpha$  and  $\gamma$ . For small  $\lambda$ , i.e. smaller than the lattice spacing  $a$ , the decay largely takes place between the first two lattice sites. We are, however, interested in systems that decay over a considerable number of lattice sites such that we are able to compare our results with a continuum system. In section 3.3 we will take a look at this continuum limit.

### 3.2 Rotation of Particle Flux

In the previous section we discussed the accumulation of particles at the wall for active systems. In this section we briefly examine another interesting phenomenon of active systems: rotation of particle flux. The particle flux is defined as the number of particles passing through a surface. In a one-dimensional system the particle flux in position space is simply the net number of particle transitions between two sites, which, of course, does not have the possibility to harbour rotation. However, examining the particle flux in position and orientation space provides the possibility of flux rotation in a one-dimensional system.

The flux  $J_{lk}$  between a state  $k = (i, e)$  and  $l = (i', e')$  is defined as the number of particles travelling from state  $k$  to  $l$  minus the number of particles travelling from  $l$  to  $k$ . Hence, in the steady state it is given by

$$J_{lk} = M_{lk}n_k - M_{kl}n_l, \quad (3.11)$$

where  $n_k$  and  $n_l$  are, respectively, the number of particles in state  $k$  and  $l$  of the steady state and  $M_{lk}$  is the probability to change from state  $k$  to state  $l$ .

During one timestep  $\tau$  particles at site  $i = 2, \dots, N - 1$  always translate to a neighbouring site  $i \pm 1$ , while particles at site  $i = 1$  and  $i = N$  have the additional possibility remain at the same lattice site, due to a collision with the wall. There are four distinct transitions from site  $i$  to  $i + 1$ , with  $i = 1, \dots, N - 1$ : (1) maintaining orientation  $+1$ , (2) maintaining orientation  $-1$ , (3) changing orientation from  $+1$  to  $-1$ , and (4) changing orientation from  $-1$  to  $+1$ . A representation of these four transitions can be seen in figure 5.

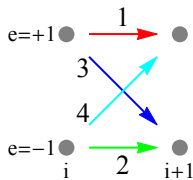


Figure 5: Representation of the four transitions from site  $i$  to site  $i + 1$ .

Using Eq.(3.11) we are able to calculate the fluxes between site  $i$  and  $i + 1$ , with  $i = 1, \dots, N - 1$ , corresponding to these four transitions

$$J_{1,i} = (1 - \gamma) \left[ \frac{1}{2}(1 + \alpha)n_{i,+} - \frac{1}{2}(1 - \alpha)n_{i+1,+} \right], \quad (3.12)$$

$$J_{2,i} = (1 - \gamma) \left[ \frac{1}{2}(1 - \alpha)n_{i,-} - \frac{1}{2}(1 + \alpha)n_{i+1,-} \right], \quad (3.13)$$

$$J_{3,i} = \frac{1}{2}(1 - \alpha)\gamma [n_{i,+} - n_{i+1,-}], \quad (3.14)$$

$$J_{4,i} = \frac{1}{2}(1 + \alpha)\gamma [n_{i,-} - n_{i+1,+}]. \quad (3.15)$$

In a passive system  $\alpha = 0$ ,  $\gamma = \frac{1}{2}$  and, due to the homogeneous distribution of particles,  $n_{i,e} = \frac{1}{2}$  for  $i = 1, \dots, N - 1$  and  $e = \pm 1$ . Hence, for a passive system  $J_1 = J_2 = J_3 = J_4 = 0$ . This, however, is not the case for an active system.

Figures 6a and 6b show the particle flux in position and orientation space at, respectively, the left and right wall of an active system with  $\alpha = 0.01$ ,  $\gamma = 0.001$  and  $N = 251$ . Figures 6c and 6d show the magnitude of the fluxes  $J_1$ ,  $J_2$ ,  $J_3$  and  $J_4$  per lattice site. Notice that in the bulk  $J_3 = J_4 = 0$  and  $J_1 = -J_2 = J_{\text{bulk}} = \frac{1}{2}\alpha(1 - \gamma) \neq 0$ , which follow from Eq.(3.12)-(3.15) and the homogeneous particle distribution of the bulk, i.e.  $n_{i,e} = \frac{1}{2}$  for  $i$  inside the bulk and  $e = \pm 1$ . In the next section we derive that  $\alpha, \gamma \downarrow 0$  in the continuum limit and that the self-propulsion velocity is given by  $v_0 = \frac{a\alpha}{\tau}$ . Hence, the magnitude of the bulk flux in the continuum limit is given by  $J_{\text{bulk}} \approx \frac{1}{2}\alpha = \frac{v_0\tau}{2a}$ . Looking at the representation of the particle flux in position and orientation space of figures 6a and 6b, it is clear to see that there is an overall (clockwise) rotation in the particle flux in position and orientation space. For active systems this rotation is always clockwise in this representation and the magnitude depends on the activity of the system.

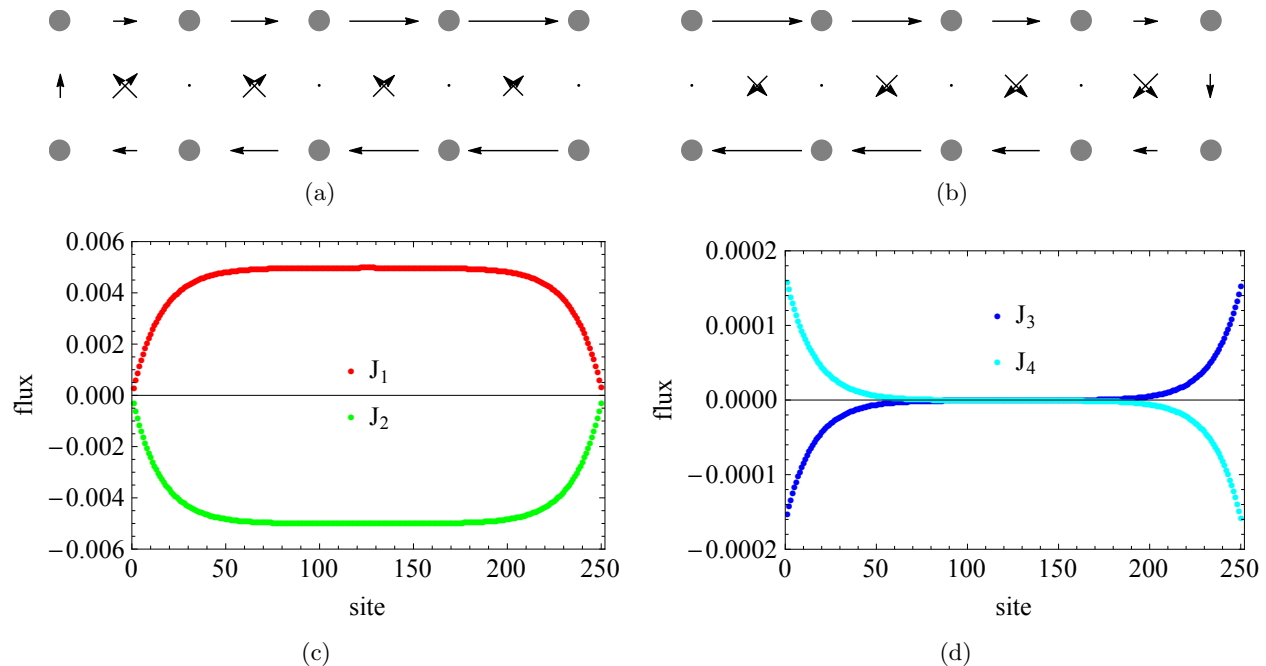


Figure 6: Particle flux in position and orientation space of (a) the 5 most left sites and (b) the 5 most right sites of an active system with  $\alpha = 0.01$ ,  $\gamma = 0.001$  and  $N = 251$ . The arrow length is a measure for flux magnitude. The arrows between different orientations, i.e. transition 3 and 4, are multiplied by a factor 2 to make them better visible. The magnitude of the fluxes  $J_1$ ,  $J_2$ ,  $J_3$  and  $J_4$  per lattice site are shown in (c) and (d).

### 3.3 Continuum Limit and Analogy with Continuous Model

In this section we take a look at the continuum limit of our lattice model and derive an analogy between our discrete model and a continuum ABP model. In a continuum model the steady state of the system is given by the probability density distribution which solves the overdamped Fokker-Planck equation (Eq.(1.9)). Recall that our lattice has  $N$  sites and lattice constant  $a$ . We define the probability density of particles with orientation  $e$  as

$$\psi_e(x, t) = \frac{n_{i,e}(t)}{a}, \quad (3.16)$$

where  $x = (i-1)a$  for  $i = 1, \dots, N$  and  $e = \pm 1$ . Using this definition, the overdamped Fokker-Planck equation for a one-dimensional system without an external potential is given by

$$\partial_t \psi_e(x, t) = -v_0 e \partial_x \psi_e(x, t) + D_t \partial_{xx} \psi_e(x, t) + \frac{D_r}{2} [\psi_{-e}(x, t) - \psi_e(x, t)], \quad (3.17)$$

where  $v_0$  is the self-propulsion velocity and  $D_t$  and  $D_r$  the translational and rotational diffusion coefficients. To derive an analogy between our discrete system and a continuum system, we first have to define the continuum limit in our system. In the continuum limit the lattice constant  $a$  should be small compared to all other length scales in the system, thus we assume  $a \sim \epsilon$  and take  $\epsilon \downarrow 0$ . Simultaneously the number of lattice sites  $N$  should go to infinity, such that  $L = (N - 1)a$  remains finite. The velocity, angular velocity, translational diffusion and rotational diffusion should also remain finite as  $\epsilon \downarrow 0$ . Using the rotation matrix equation Eq.(2.2) and translation equations Eq.(3.1) and Eq.(3.2) we find

$$\begin{aligned} \frac{\langle \Delta x \rangle_{i,e}}{\tau} &= e(1 - 2\gamma) \frac{\alpha a}{\tau}, & \frac{\langle e(t + \tau) - e(t) \rangle_{i,e}}{\tau} &= \frac{2\gamma}{\tau}, \\ \frac{\langle (\Delta x)^2 \rangle_{i,e}}{\tau} &= \frac{a^2}{\tau}, & \frac{\langle (e(t + \tau) - e(t))^2 \rangle_{i,e}}{\tau} &= \frac{4\gamma}{\tau}, \end{aligned}$$

where  $\frac{\langle \Delta x \rangle_{i,e}}{\tau}$  is the velocity,  $\frac{\langle e(t + \tau) - e(t) \rangle_{i,e}}{\tau}$  the angular velocity, and  $\frac{\langle (\Delta x)^2 \rangle_{i,e}}{\tau}$  and  $\frac{\langle (e(t + \tau) - e(t))^2 \rangle_{i,e}}{\tau}$ , respectively, the translational and rotational diffusion.

Keeping in mind that we already assumed  $a \sim \epsilon$ , we deduce  $\gamma \sim \tau \sim \epsilon^2$  and  $\alpha \sim \epsilon$  using the fact that the above quantities should remain finite when  $\epsilon \downarrow 0$ . Thus, we see that in the continuum limit  $\alpha, \gamma \downarrow 0$ , which is in agreement with our findings of the previous section, namely, that the decay length  $\lambda$  is large for small  $\alpha$  and  $\gamma$ .

Now that we know what the continuum limit implies, we need to find an analogy between the discrete and continuum model by finding expressions for  $v_0$ ,  $D_r$  and  $D_t$  in terms of  $a$ ,  $\tau$ ,  $\alpha$  and  $\gamma$ . To do this we derive the Fokker-Planck equation starting from our translation and rotation matrices. First we rescale our variables  $\tilde{a} = \frac{a}{\epsilon}$ ,  $\tilde{\alpha} = \frac{\alpha}{\epsilon}$ ,  $\tilde{\gamma} = \frac{\gamma}{\epsilon^2}$  and  $\tilde{\tau} = \frac{\tau}{\epsilon^2}$  and express the translation and rotation matrices of Eq.(2.3) and Eq.(3.8) in the form

$$T_{(i_2, e_2 | i_1, e_1)} = \delta_{e_2, e_1} \left[ \frac{1}{2}(1 + \epsilon \tilde{\alpha} e) \delta_{i_2, i_1 + 1} + \frac{1}{2}(1 - \epsilon \tilde{\alpha} e) \delta_{i_2, i_1 - 1} \right], \quad (3.18)$$

$$R_{(i_2, e_2 | i_1, e_1)} = \delta_{i_2, i_1} \left[ (1 - \epsilon^2 \tilde{\gamma}) \delta_{e_2, e_1} + \epsilon^2 \tilde{\gamma} \delta_{e_2, -e_1} \right], \quad (3.19)$$

where  $T_{(i_2, e_2 | i_1, e_1)}$  and  $R_{(i_2, e_2 | i_1, e_1)}$  are the translation and rotation matrix elements corresponding to the probability of going from state  $n_{(i_1, e_1)}$  to  $n_{(i_2, e_2)}$ .

Now, using the expansion

$$\delta_{i_2, i_1 \pm 1} - \delta_{i_2, i_1} = \mp \epsilon \tilde{a} \partial_x + \frac{1}{2} \epsilon^2 \tilde{a}^2 \partial_{xx} + \mathcal{O}(\epsilon^3), \quad (3.20)$$

we rewrite Eq.(3.18) to find

$$T_{(i_2, e_2 | i_1, e_1)} = \delta_{i_2, i_1} \delta_{e_2, e_1} + \epsilon^2 \delta_{e_2, e_1} \left[ -e \tilde{\alpha} \tilde{a} \partial_x + \frac{1}{2} \tilde{a}^2 \partial_{xx} \right] + \mathcal{O}(\epsilon^3) \quad (3.21)$$

and restate this equation and Eq.(3.19) to get

$$T = \mathbb{1} + \epsilon^2 T^{(2)} + \mathcal{O}(\epsilon^3), \quad (3.22)$$

$$R = \mathbb{1} + \epsilon^2 R^{(2)}, \quad (3.23)$$

with  $T_{e_2, e_1}^{(2)} = \delta_{e_2, e_1} (-e \tilde{\alpha} \tilde{a} \partial_x + \frac{1}{2} \tilde{a}^2 \partial_{xx})$  and  $R_{e_2, e_1}^{(2)} = \tilde{\gamma} (\delta_{e_2, -e_1} - \delta_{e_2, e_1})$ .

To arrive at the Fokker-Planck equation from Eq.(3.17) we use

$$\frac{|n(t + \tau)\rangle - |n(t)\rangle}{\tau} = \frac{M|n(t)\rangle - |n(t)\rangle}{\tau}. \quad (3.24)$$

Equivalently, from Eq.(3.16) we have

$$\frac{|\psi(x, t + \tau)\rangle - |\psi(x, t)\rangle}{\tau} = \frac{(TR - \mathbb{1})}{\tau} |\psi(x, t)\rangle, \quad (3.25)$$

where  $|\psi\rangle = (\psi_+, \psi_-)^T$  with  $\pm$  indicating the orientation. Now, substituting Eq.(3.22) and Eq.(3.23) into Eq.(3.25) we get

$$\partial_t \psi_e(x, t) + \mathcal{O}(\epsilon^2) = \left( \frac{T^{(2)}}{\tilde{\tau}} + \frac{R^{(2)}}{\tilde{\tau}} \right) \psi_e(x, t) + \mathcal{O}(\epsilon^2), \quad (3.26)$$

and taking the limit  $\epsilon \downarrow 0$  gives

$$\partial_t \psi_e(x, t) = -e \lim_{\epsilon \downarrow 0} \left( \frac{\tilde{\alpha} \tilde{a}}{\tilde{\tau}} \right) \partial_x \psi_e(x, t) + \frac{1}{2} \lim_{\epsilon \downarrow 0} \left( \frac{\tilde{\alpha}^2}{\tilde{\tau}} \right) \partial_{xx} \psi_e(x, t) + \lim_{\epsilon \downarrow 0} \left( \frac{\tilde{\gamma}}{\tilde{\tau}} \right) [\psi_{-\epsilon}(x, t) - \psi_e(x, t)]. \quad (3.27)$$

Comparing this to the Fokker-Planck equation of Eq.(3.17) we find

$$v_0 \equiv \lim_{\epsilon \downarrow 0} \left( \frac{\tilde{a} \tilde{\alpha}}{\tilde{\tau}} \right) = \lim_{\epsilon \downarrow 0} \left( \frac{a\alpha}{\tau} \right), \quad (3.28)$$

$$D_t \equiv \lim_{\epsilon \downarrow 0} \left( \frac{\tilde{a}^2}{2\tilde{\tau}} \right) = \lim_{\epsilon \downarrow 0} \left( \frac{a^2}{2\tau} \right), \quad (3.29)$$

$$D_r \equiv \lim_{\epsilon \downarrow 0} \left( \frac{2\tilde{\gamma}}{\tilde{\tau}} \right) = \lim_{\epsilon \downarrow 0} \left( \frac{2\gamma}{\tau} \right), \quad (3.30)$$

where the limit  $\epsilon \downarrow 0$  is to be interpreted as the limit in which the lattice constant is small compared to the other length scales in the system.

### 3.4 One-Dimensional Solutions of the Fokker-Planck Equation

Having derived the analogy between the discrete and continuum model in the previous section, we solve the Fokker-Planck equation in this section to find an expression for the steady state density and polarisation distributions and compare these distributions with our numerical distributions in the next section.

Equivalently to Eq.(2.15), the density and polarisation are defined by

$$\rho(x, t) = \psi_+(x, t) + \psi_-(x, t), \quad m(x, t) = \psi_+(x, t) - \psi_-(x, t). \quad (3.31)$$

Using the Fokker-Planck equation, Eq.(3.17), we derive the differential equations for the density and polarisation

$$\partial_t \rho(x, t) = -\partial_x [v_0 m(x, t) - D_t \partial_x \rho(x, t)], \quad (3.32)$$

$$\partial_t m(x, t) = -\partial_x [v_0 \rho(x, t) - D_t \partial_x m(x, t)] - D_r m(x, t). \quad (3.33)$$

In the stationary state, i.e.  $\partial_t \rho(x, t) = \partial_t m(x, t) = 0$ , Eq.(3.32) and Eq.(3.33) can be rewritten into

$$\partial_x \rho(x) = \frac{\text{Pe}^2}{L_2^2} m(x), \quad (3.34)$$

$$\partial_{xx} m(x) = \frac{1}{\lambda^2} m(x), \quad (3.35)$$

where Péclet number  $\text{Pe}$ , which is a measure for the activity of the system, is defined as

$$\text{Pe} = \frac{L_1}{L_2} = \frac{v_0}{\sqrt{D_t D_r}}, \quad (3.36)$$

and  $L_1$ ,  $L_2$  and  $\lambda$  are length scales given by

$$L_1 = \frac{v_0}{D_r}, \quad (3.37)$$

$$L_2 = \sqrt{\frac{D_t}{D_r}}, \quad (3.38)$$

$$\lambda = \frac{L_2}{\sqrt{1 + \text{Pe}^2}}. \quad (3.39)$$

The first length scale  $L_1$  is called the ‘‘swimmers’ run length’’. It is a measure for the distance an ABP travels before changing direction [29]. The second length scale  $L_2$  measures the translational diffusion and  $\lambda$ , as already mentioned in section 3.1, is the decay length of the accumulation at the wall.

For the solutions of the differential equations Eq.(3.34) and Eq.(3.35) we look at two different systems: a system with one wall and a system with two walls. In a one-dimensional system with one wall at  $x = 0$  we have boundary conditions

$$\lim_{x \rightarrow \infty} m(x) = 0, \quad (3.40)$$

$$\lim_{x \rightarrow \infty} \rho(x) = \rho_{\text{bulk}}. \quad (3.41)$$

The general solution of Eq.(3.35) is given by

$$m(x) = c_1 e^{x/\lambda} + c_2 e^{-x/\lambda}, \quad (3.42)$$

where  $c_1$  and  $c_2$  are constants. Applying the first boundary condition, i.e. Eq.(3.40), on Eq.(3.42) we find  $c_1 = 0$  and  $c_2 = m(x=0) = m_0$ . Now, using this, Eq.(3.34) and the second boundary condition we find

$$\rho(x) = -m_0 \lambda \frac{\text{Pe}^2}{L^2} e^{-x/\lambda} + \rho_{\text{bulk}}. \quad (3.43)$$

Furthermore, we can use that there should be no flux at  $x = 0$ , i.e.  $[v_0 \rho(x) - D_t \partial_x m(x)]_{x=0} = 0$ , to find

$$m_0 = -\rho_{\text{bulk}} \text{Pe} \sqrt{1 + \text{Pe}^2}. \quad (3.44)$$

Finally, by substituting Eq.(3.44) we get the solution for the density and polarisation distribution in a one-dimensional system with one wall

$$\rho_{1\text{w}}(x) = \rho_{\text{bulk}} \left( 1 + \text{Pe}^2 e^{-x/\lambda} \right), \quad (3.45)$$

$$m_{1\text{w}}(x) = -\rho_{\text{bulk}} \text{Pe} \sqrt{1 + \text{Pe}^2} e^{-x/\lambda}. \quad (3.46)$$

Notice that Eq.(3.45) and Eq.(3.46) are in accordance with the observed distributions Eq(3.9) and Eq.(3.10). For the one-dimensional system with two walls, one at  $x = 0$  and one at  $x = L$ , we have the boundary condition  $m(x=0) = -m(x=L) = m_0$ . Applying this condition on the general solution given by Eq.(3.42) we find  $c_1 = m_0 \frac{1}{1 - e^{L/\lambda}}$  and  $c_2 = m_0 \frac{-e^{L/\lambda}}{1 - e^{L/\lambda}}$ . Substituting this back into Eq.(3.42) and using Eq.(3.34) we find

$$m(x) = m_0 \frac{e^{x/\lambda} - e^{\frac{L-x}{\lambda}}}{1 - e^{L/\lambda}}, \quad (3.47)$$

$$\rho(x) = \rho_{\text{bulk}} + m_0 \frac{\text{Pe}}{\sqrt{1 + \text{Pe}^2}} \frac{e^{x/\lambda} + e^{\frac{L-x}{\lambda}}}{1 - e^{L/\lambda}}. \quad (3.48)$$

Again, we use the fact that there is no flux at  $x = 0$  to find  $m_0 = \rho_{\text{bulk}} \text{Pe} \sqrt{1 + \text{Pe}^2} \frac{1 - e^{x/\lambda}}{1 + e^{L/\lambda}}$  and after substituting this back into Eq.(3.47) and Eq.(3.48) we find our solution for the density and polarisation distribution in a one-dimensional system with two walls

$$\rho_{2\text{w}}(x) = \rho_{\text{bulk}} \left( 1 + \text{Pe}^2 \frac{\sinh \frac{x}{\lambda} + \sinh \frac{L-x}{\lambda}}{\sinh \frac{L}{\lambda}} \right), \quad (3.49)$$

$$m_{2\text{w}}(x) = \rho_{\text{bulk}} \text{Pe} \sqrt{1 + \text{Pe}^2} \frac{\cosh \frac{x}{\lambda} - \cosh \frac{L-x}{\lambda}}{\sinh \frac{L}{\lambda}}. \quad (3.50)$$

The density at the centre of the system is given by  $\rho_c = \rho_{2\text{w}}(x = \frac{L}{2}) = \rho_{\text{bulk}} \left( 1 + 2\text{Pe}^2 \frac{\sinh \frac{L}{2\lambda}}{\sinh \frac{L}{\lambda}} \right)$ . Notice that  $\rho_c \geq \rho_{\text{bulk}}$ . In the limit  $L \gg \lambda$  we see that  $\rho_{2\text{w}}(x) \rightarrow \rho_{1\text{w}}(x)$  and  $m_{2\text{w}}(x) \rightarrow m_{1\text{w}}(x)$  for  $x \leq \frac{L}{2}$ .



### 3.5 Wall Pressure

Using the expressions for the density distribution derived in the previous section, i.e. Eq.(3.45) and Eq.(3.49), it is straightforward to find the wall pressure of the system. Let us define the pressure on the wall as

$$\Pi_w = \rho_w k_B T, \quad (3.51)$$

where  $\rho_w$  is the density at the wall [29]. In an active system the wall pressure then consists of the osmotic pressure of the Brownian particles, i.e. the pressure  $\rho_{\text{bulk}} k_B T$  in a passive system, and the so-called swim pressure, which is the pressure caused by the self-propulsion of the particles. We can therefore rewrite equation Eq.(3.51) as

$$\Pi_w = \rho_{\text{bulk}} k_B T_{\text{eff}} = \rho_{\text{bulk}} k_B (T + T_s), \quad (3.52)$$

where  $T_{\text{eff}}$  is the effective temperature and  $T_s$  the additional swim temperature.

Using Eq.(3.45) and Eq.(3.49) we find  $\rho_w = \rho_{\text{bulk}} (1 + \text{Pe}^2)$  for both the one- and two-wall system. Thus, the swim temperature is given by

$$T_s = \text{Pe}^2 T. \quad (3.53)$$

It is noteworthy that the density at the wall and, hence, the pressure only depend on the activity of the system and not on other properties, such as the number of walls or the distance between two walls. The reason for this lies in our consideration of non-interacting particles and hard wall potentials.

### 3.6 Comparison with Continuum Model

In section 3.4 we introduced the length scales  $L_1$  and  $L_2$ , and the Péclet number  $\text{Pe}$  to find the continuum descriptions of the density and polarisation distribution for a one-dimensional system. Now, using Eq.(3.28)-(3.30) and Eq.(3.36)-(3.39), we express  $L_1$ ,  $L_2$ ,  $\lambda$  and  $\text{Pe}$  in terms of our discrete model variables

$$L_1 = \lim_{\epsilon \downarrow 0} \left( \frac{a\alpha}{2\gamma} \right), \quad (3.54)$$

$$L_2 = \lim_{\epsilon \downarrow 0} \left( \frac{a}{2\sqrt{\gamma}} \right), \quad (3.55)$$

$$\text{Pe} = \lim_{\epsilon \downarrow 0} \left( \frac{\alpha}{\sqrt{\gamma}} \right), \quad (3.56)$$

$$\lambda = \lim_{\epsilon \downarrow 0} \left( \frac{a}{2\sqrt{\gamma(1 + \alpha^2/\gamma)}} \right). \quad (3.57)$$

To compare the continuum findings of section 3.4 to our discrete model we calculate the density and polarisation distribution for different Péclet numbers. For this we fix  $\alpha$  and for fixed  $\text{Pe}$  calculate  $\gamma$  using Eq.(3.56). We then use Eq.(3.45) and Eq.(3.46) to fit the distributions to the one-wall model and Eq.(3.49) and Eq.(3.50) to fit it to the two-wall model. Figure 7 shows the  $\text{Pe}$  dependence of the decay length  $\lambda$  and the density and polarisation prefactors,  $\text{Pe}^2$  and  $\text{Pe}\sqrt{1 + \text{Pe}^2}$ , for  $\alpha = 0.005$  and  $\alpha = 0.01$ . The filled markers correspond to data obtained by fitting to the one-wall model and the empty markers to the two-wall model. The black lines depict the expected continuum values. All results are obtained using a lattice of  $N = 251$  sites.

The grey horizontal lines of figure 7a correspond to  $\frac{\lambda}{a} = 8$  and  $\frac{\lambda}{a} = 23$  and the dashed vertical lines in figure 7a and 7b indicate the Péclet numbers belonging to these values of  $\frac{\lambda}{a}$ . We clearly see that the data of figure 7b differ from the expected continuum value, both for the one- and two-wall model, for  $\frac{\lambda}{a} < 8$ . This is due to the fact that  $\frac{\lambda}{a} < 8$  falls outside the continuum limit. For  $\frac{\lambda}{a} > 23$  the data belonging to the one-wall model starts to deviate from the continuum line, while the data belonging to the two-wall model does agree with the continuum line. This is explained by the fact that for  $\frac{L}{\lambda} \lesssim 10$  the decay of the particle accumulation at the walls is not fast enough for the one-wall model, causing the particles on the left side of the system to also feel the presence of the right wall and vice versa. Using Eq.(3.45) we see that accumulation of a system with  $\frac{L}{\lambda} = 10$  has only decayed with a factor  $e^{-5} \approx 1/150$  at  $x = \frac{L}{2}$ . Thus, the effect of both walls is considerable

at the middle most site of the system. Hence, systems with  $\frac{L}{\lambda} \gtrsim 10$  must be compared to the two-wall model and cannot be approximated with the one-wall model.

The failure of the one-wall approximation for small  $\frac{L}{\lambda}$  can also be seen in figures 7c and 7d.

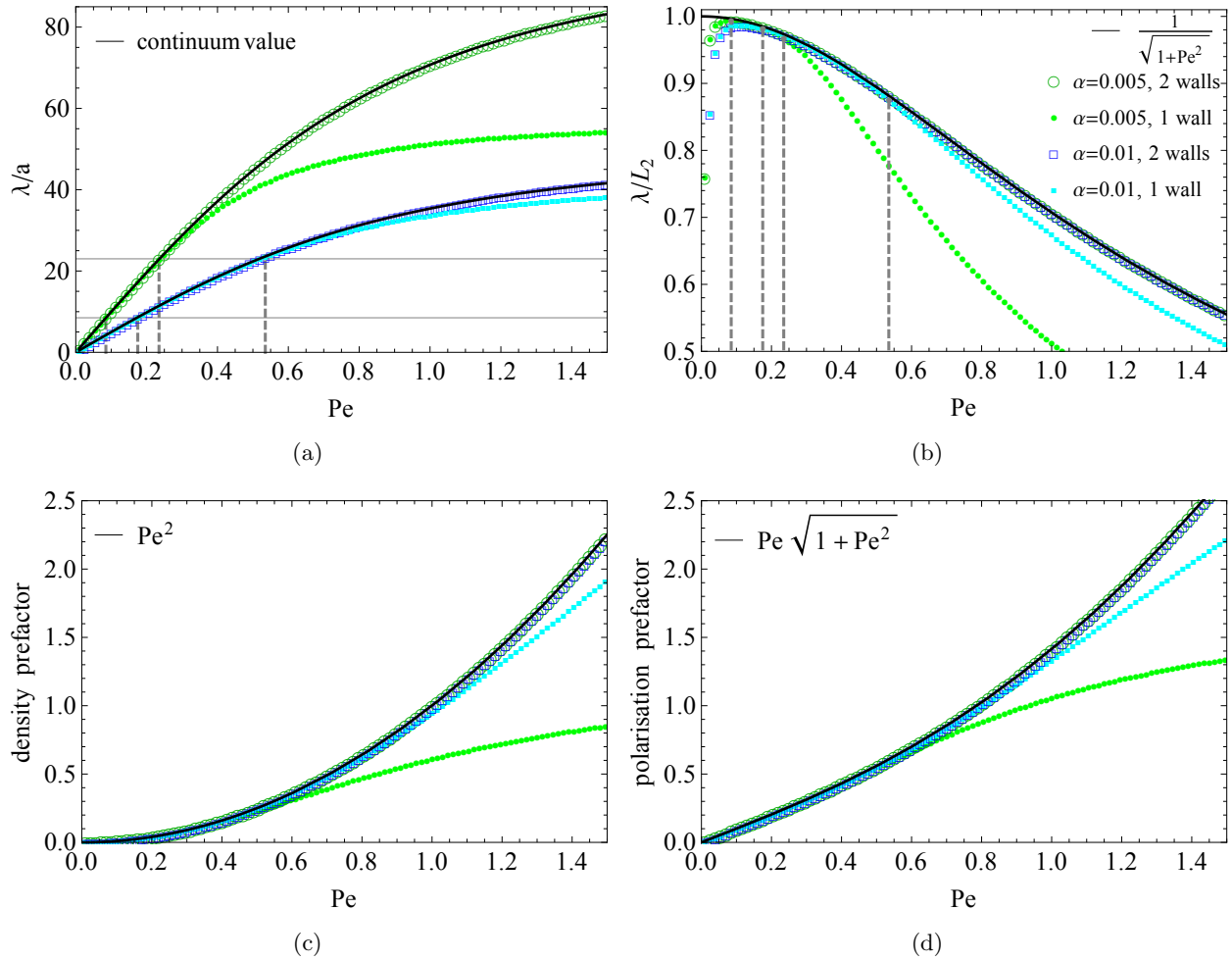


Figure 7: Dependence on the Péclet number  $Pe$  of (a) the decay length  $\lambda$  scaled by the lattice constant  $a$ , (b)  $\lambda$  scaled by the translational diffusion length scale  $L_2$  and the prefactors of (c) the density and (d) polarisation distribution, i.e.  $Pe^2$  and  $Pe\sqrt{1+Pe^2}$ , for  $\alpha = 0.005$  and  $\alpha = 0.01$ . The black lines depict the expected continuum values. The grey horizontal lines of (a) correspond to  $\frac{\lambda}{a} = 8$  and  $\frac{\lambda}{a} = 23$  and the dashed vertical lines in (a) and (b) indicate the Péclet numbers belonging to these values for  $\frac{\lambda}{a}$ . All results are obtained using a lattice of  $N = 251$  sites.

## 4 Two-Parameter Model with Ratchet Potential

Thus far, we only considered systems without any external potentials, except the hard wall boundaries. However, interesting phenomena arise when we consider the presence a non-zero external potential. In this chapter we investigate the influence of a ratchet potential on the steady state distributions by adjusting our two-parameter model of the previous chapter.

We consider ratchet potentials of the form

$$V(x) = \begin{cases} 0 & \text{for } x < x_0 - x_L, \\ \frac{V_{\max}}{x_L}(x - x_0 + x_L) & \text{for } x_0 - x_L \leq x \leq x_0, \\ \frac{V_{\max}}{x_R}(x_0 + x_R - x) & \text{for } x_0 \leq x \leq x_0 + x_R, \\ 0 & \text{for } x > x_0 + x_R, \end{cases} \quad (4.1)$$

where  $V_{\max}$  is the ratchet height,  $x_0$  the location of the top of the ratchet and  $x_L$  and  $x_R$ , respectively, the length of the left and right side of the ratchet.

A representation of this ratchet potential is given by the dashed line in figure 8. The solid line represents the density distribution of the steady state of a passive system, which, as mentioned in section 1.1, is given by a Boltzmann distribution, i.e. Eq.(1.7). Notice that the presence of the ratchet potential divides the system into two subsystems each with their own bulk density. We indicate the bulk density of the left subsystem with  $\rho_L$  and of the right subsystem with  $\rho_R$ . In a passive system  $\rho_L = \rho_R$ , as the density distribution is given by  $\rho(x) = \rho_{\text{bulk}}e^{-\beta V(x)}$  and  $V(x) = 0$  in both the bulk of the left and right subsystem. However, for an active system the bulk density belonging to the steepest side of the ratchet turns out to be higher than the bulk density belonging to the more gentle side in a steady state. This inequality in the bulk densities is explained by the fact that active particles, due to their propulsion force, are able to cross the potential barrier more easily from the more gentle side than from the steeper side. Thus, in order to compensate for the reduced transition probability per particle at the steeper side, a higher density develops on this side of the ratchet in the steady state.

In this thesis we only consider ratchet potentials with  $x_R \leq x_L$ , such that  $\rho_R \geq \rho_L$ . We can take this restriction without loss of generality due to the symmetry of our model: a system with  $x'_R \geq x'_L$  is simply the mirror image of a system with  $x_R = x'_L$  and  $x_L = x'_R$ .

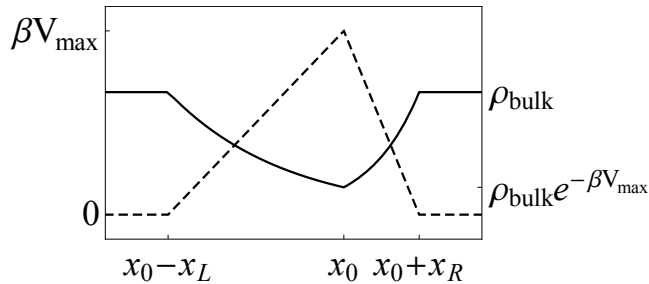


Figure 8: The dashed line represents the ratchet potential  $\beta V(x)$  of Eq.(4.1) and the solid line the density distribution of the steady state of a passive system, i.e.  $\rho(x) = \rho_{\text{bulk}}e^{-\beta V(x)}$ . The top of the ratchet is positioned at  $x_0$  and has the value  $\beta V_{\max}$ . The length of the left and right side of the ratchet are  $x_L$  and  $x_R$ , respectively.

### 4.1 Ratchet Force and Time Evolution of a State

The force on a particle due to an external potential is given by  $\vec{F}(\vec{r}) = -\nabla V(\vec{r})$ . Discretised and for one-dimension this is equivalent to

$$F_i = -\frac{V_{i+1} - V_{i-1}}{2}, \quad (4.2)$$

where  $F_i$  and  $V_i$  are, respectively, the scaled force and potential at site  $i$ . The force is scaled with the lattice constant  $a$ , such that  $F_i$  has the dimension of energy and  $\beta F_i$ , where  $\beta = 1/k_B T$ , is dimensionless.

Using Eq.(4.1) we find the discretised ratchet force

$$F_i = \begin{cases} \frac{F_L}{2} & \text{for } i = i_0 - i_L, \\ F_L & \text{for } i_0 - i_L < i < i_0, \\ \frac{F_L + F_R}{2} & \text{for } i = i_0, \\ F_R & \text{for } i_0 < i < i_0 + i_R, \\ \frac{F_R}{2} & \text{for } i = i_0 + i_R, \\ 0 & \text{elsewhere,} \end{cases} \quad (4.3)$$

with  $F_L = -\frac{V_{\max}}{i_L}$  and  $F_R = \frac{V_{\max}}{i_R}$ , respectively, the force on the left and right side of the ratchet,  $i_0 = x_0/a + 1$  the lattice site on which the top of the ratchet is located and  $i_L = x_L/a$  and  $i_R = x_R/a$ , respectively, the length of the left and right side of the ratchet in terms of the lattice spacing.

The potential has no effect on the rotational step, but in the translational step it results in an additional probability term proportional to the force for the particles travelling to the right and proportional to minus the force for particles travelling to the left. We therefore adjust the translational equations of section 3.1 with an additional force term

$$n_{i,-}(t + \tau) = \left( \frac{1 + \alpha}{2} - \frac{\beta F_{i+1}}{4} \right) n'_{i+1,-}(t) + \left( \frac{1 - \alpha}{2} + \frac{\beta F_{i-1}}{4} \right) n'_{i-1,-}(t), \quad (4.4)$$

$$n_{i,+}(t + \tau) = \left( \frac{1 + \alpha}{2} + \frac{\beta F_{i-1}}{4} \right) n'_{i-1,+}(t) + \left( \frac{1 - \alpha}{2} - \frac{\beta F_{i+1}}{4} \right) n'_{i+1,+}(t). \quad (4.5)$$

The necessity of the factor  $1/4$  shows itself when taking the continuum limit.<sup>3</sup>

Using the translation equations (Eq.(4.4) and Eq.(4.5)) and the definition for  $F_i$  (Eq.(4.2)) we construct the new translation matrix  $T^{\text{rat}}$ . The transition matrix is given by  $M^{\text{rat}} = T^{\text{rat}}R$ , with  $R$  given by Eq.(2.2). We once again find the steady state by calculating the eigenvector of  $M^{\text{rat}}$  belonging to the eigenvalue equal to 1 and rescale the vector such that  $\rho_L = 1$ .

Unfortunately, for passive systems, i.e.  $\alpha = 0$  and  $\gamma = \frac{1}{2}$ , we find steady states with  $\rho_R \neq \rho_L$ . Depending on the shape of the ratchet the relative difference usually has an order  $10^{-4} - 1$ . However, for very steep ratchets it can even reach on order of  $10^2$  or higher. The inequality of the bulk densities in passive systems is caused by small errors due to the discretisation of the ratchet force. Using detailed balance, which states that each elementary process of a system in equilibrium should be equilibrated by its reverse process, we write  $n_{i_1, e_1} M_{(i_2, e_2 | i_1, e_1)}^{\text{rat}} = n_{i_2, e_2} M_{(i_1, e_1 | i_2, e_2)}^{\text{rat}}$ . This can be rewritten to  $\rho_{i_1} T_{(i_2 | i_1)}^{\text{rat}} = \rho_{i_2} T_{(i_1 | i_2)}^{\text{rat}}$  for a passive system. Thus, we find  $\rho_{i_2} = \rho_{i_1} \frac{T_{(i_2 | i_1)}^{\text{rat}}}{T_{(i_1 | i_2)}^{\text{rat}}}$  and use this to iterate from  $\rho_{i_1} = \rho_L$  to  $\rho_{i_2} = \rho_R$  to find the bulk density ratio

$$\frac{\rho_R}{\rho_L} = \underbrace{\left( \frac{\frac{1}{2} + \frac{\beta F_L}{8}}{\frac{1}{2} - \frac{\beta F_L}{8}} \right) \left( \frac{\frac{1}{2} + \frac{\beta F_R}{8}}{\frac{1}{2} - \frac{\beta F_R}{8}} \right) \left( \frac{\frac{1}{2} + \frac{\beta F_L}{4}}{\frac{1}{2} - \frac{\beta F_L}{4}} \right)^{i_L - 1} \left( \frac{\frac{1}{2} + \frac{\beta F_R}{4}}{\frac{1}{2} - \frac{\beta F_R}{4}} \right)^{i_R - 1}}_A \left( \frac{\frac{1}{2} + \frac{\beta(F_L + F_R)}{8}}{\frac{1}{2} - \frac{\beta(F_L + F_R)}{8}} \right). \quad (4.6)$$

In the continuum limit  $i_L, i_R \rightarrow \infty$  we clearly have  $F_L, F_R \downarrow 0$ , and Eq.(4.6) yields indeed  $\frac{\rho_R}{\rho_L} = 1$ . To ensure that  $\frac{\rho_R}{\rho_L} = 1$  in the non-continuum limit we make a small correction in the definition of the force at the top of the ratchet. Instead of  $F_{i_0} = \frac{F_L + F_R}{2}$ , we use  $F_{i_0, \text{cor}} = \frac{2}{\beta} \frac{1-A}{1+A}$ . Since  $A \approx 1$  for a ‘‘decent’’-sized ratchet, i.e. a ratchet with  $i_R, i_L \gtrsim 20$ , the corrected force  $\beta |F_{i_0, \text{cor}}| \ll 1$ . Thus, the correction is indeed small.

## 4.2 Examples of Steady States

In this section we use the matrix  $M^{\text{rat}}$  derived in the previous section to calculate the steady states of a few active systems. However, before we look at some examples of steady state distributions, we first have to define two restrictions of our model. The first restriction considers the ratchet size: each side of the ratchet should consist of a considerable number of lattice sites, such that the continuum limit holds and the forces due to the ratchet are reasonably small. By trial and error we find that  $i_R, i_L \gtrsim 20$  is usually large enough,

<sup>3</sup>See appendix B for the detailed calculation of this continuum limit.

but to be safe we use  $i_R, i_L \geq 40$  whenever possible. However, in the case of extremely high potentials, i.e.  $\beta V_{\max} > 15$ , one should consider a finer discretisation for the ratchet.

The second restriction considers the decay length  $\lambda$ . For a system of length  $L$  and with a ratchet potential with sides  $x_R$  and  $x_L$  the decay length is approximately restricted to the range  $[8a, \frac{L-x_R-x_L}{20}]$ . The upper bound of the range can be explained with the decay of the accumulations. A system with a ratchet potential between two hard walls forms accumulations of particles at the walls, but also at the edges of the ratchet. For the system to have a well-defined left and right bulk, these accumulations should decay fast, such that the particles in the bulk do not feel the presence of the neighbouring accumulations. We saw in section 3.6 that systems with no external potential and  $\frac{L}{\lambda} > 10$  can be approximated with the one-wall model and thus have a reasonably large bulk. Therefore, we use as a rule of thumb that  $\lambda$  should be at least ten times smaller than the distance between the wall and the edge of the ratchet. This is captured approximately by  $\lambda < \frac{L-x_R-x_L}{20}$ . The lower bound of the range can be explained by another finding in section 3.6, namely that  $\frac{\lambda}{a} > 8$  for the continuum limit to hold. However, the strictness of this bound depends on the quantity which one wants to obtain from the steady state distribution. Using, for example, the same data from section 3.6 we see that the calculated prefactors only start to deviate from the expected continuum value when  $\frac{\lambda}{a} < 2$ . We therefore use systems with  $\frac{\lambda}{a} > 8$  when possible, but also use systems with smaller  $\frac{\lambda}{a}$  when necessary and possible for the measured quantity.

Applying the two restrictions of our ratchet model, we now look at a few examples of steady state distributions. Figure 9 shows the steady state distributions for a system of  $N = 1400$  sites for Péclet numbers 1, 2, 3 and 4. The external ratchet potential is indicated by the dashed black line and has height  $\beta V_{\max} = 4$  and the length of the right and left side are, respectively,  $x_R = 40a$  and  $x_L = 160a$ . The solid black line depicts the Boltzmann distribution, i.e. the density distribution of a passive system, and the length scale  $L_2 = 40a$  for all four distributions. Using Eq.(3.39) we find  $\frac{\lambda}{a}$  is equal to  $\frac{40}{\sqrt{2}}$ ,  $\frac{40}{\sqrt{5}}$ ,  $\frac{40}{\sqrt{10}}$  and  $\frac{40}{\sqrt{17}}$  for Péclet numbers 1, 2, 3 and 4, respectively, which lie in our restricted range for  $\lambda$ . The density distributions clearly differ from the Boltzmann distribution and show inequalities of the bulk densities, i.e.  $\rho_R > \rho_L$ . Notice that the steady state belonging to  $Pe = 2$  has the greatest  $\rho_R$ . Apparently,  $\rho_R$  does not simply increase with increasing  $Pe$  as one would naively expect. In the next section we examine the dependency of the bulk density difference on the Péclet number and other variables. Also notice that the density distribution on the ratchet is quite similar to the Boltzmann distribution for  $Pe = 1$ , but increases for increasing  $Pe$ . This can be explained by the fact that particles with a low Péclet number have a low activity and therefore have a similar distribution to that of passive particles, while particles with a higher  $Pe$  have a higher activity and are therefore less hindered by the ratchet potential, which results in a higher particle density on the ratchet.

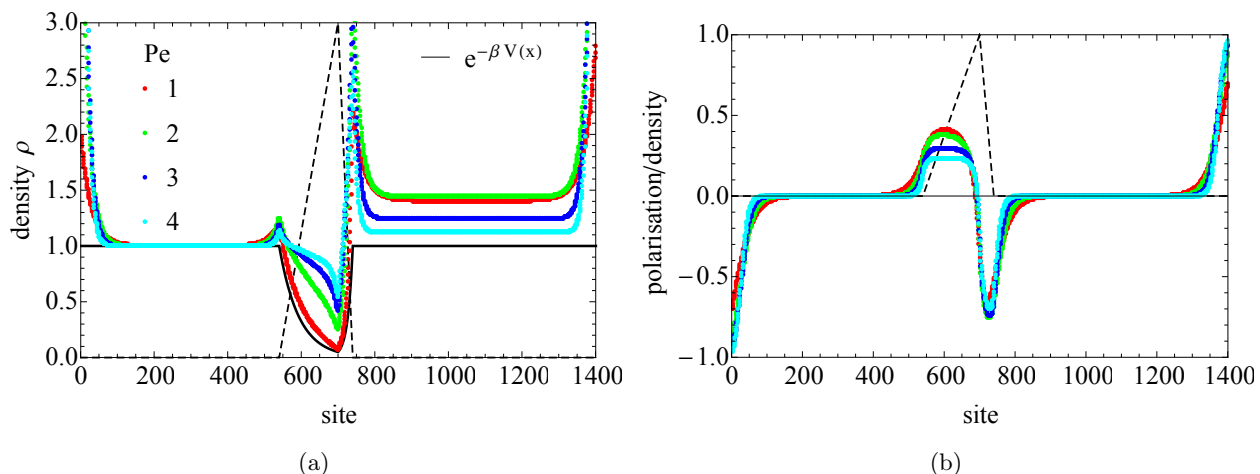


Figure 9: The density and polarisation distribution of the steady state for Péclet numbers 1, 2, 3 and 4. The polarisation distribution is divided by the density distribution. The dashed black line represents the ratchet potential and the solid black line depicts the Boltzmann distribution. The results are obtained using a lattice of  $N = 1400$  sites, translational diffusion length  $L_2 = 40a$ , and a ratchet potential with height  $\beta V_{\max} = 4$  and right and left side  $x_R = 40a$  and  $x_L = 160a$ , respectively.

Furthermore, we clearly see accumulations of particles at the walls and edges of the ratchet, all with a net polarisation in the direction of the nearest wall or ratchet edge. The net polarisation of the bulks is zero, as expected. The accumulation at the edges of the ratchet can be explained by the effect the ratchet has on the translation probabilities. The probability to translate up the ratchet is lowered, while the probability to translate down the ratchet is increased. This effect can surpass the translational preference due to the orientation of the particles, which causes particles to translate down the ratchet even though their orientation points upwards the ratchet. Once the particles arrive back at the base of the ratchet, they still have an orientation pointing towards the ratchet and thus restart their battle to cross the ratchet. This process causes many particles to get temporarily stuck at the base of the ratchet and thus an accumulation forms. Notice that the accumulation at the steep side of the ratchet is larger than the accumulation at the more gentle side. This is simply explained by the fact that the more gentle side is easier to cross than the steep side, thus particles at the steep side are stuck for a longer period of time before crossing the ratchet. The decay lengths of the accumulations at the walls are not affected by the ratchet potential: they are still given by the one-wall solutions Eq.(3.45) and Eq.(3.46) with  $\rho_{\text{bulk}}$  given by  $\rho_L$  or  $\rho_R$ . The accumulations at the edges of the ratchet decay into the bulk with a decay length equal to  $\lambda$ , which therefore appears to be a universal length scale of the problem.

### 4.3 Bulk Density Difference

The steady state density distributions displayed in figure 9a clearly show a difference in bulk densities for active systems with a ratchet potential. As already mentioned, this difference is dependent on the Péclet number. In this section we look at the difference in the bulk densities  $\frac{\rho_R}{\rho_L} - 1$  and its dependency on the four system variables. The first variable is the Péclet number  $Pe$  and the remaining three define the ratchet potential: the height  $\beta V_{\text{max}}$ , the dimensionless length of the right side  $\frac{x_R}{L_2}$  and the asymmetry of the ratchet  $\frac{x_L}{x_R} - 1$ . Figure 10 shows the bulk density difference  $\frac{\rho_R}{\rho_L} - 1$  plotted against  $Pe$ ,  $\beta V_{\text{max}}$ ,  $\frac{x_R}{L_2}$  and  $\frac{x_L}{x_R} - 1$ , all with logarithmic horizontal and vertical axes. Notice that all figures have a regime in which the data can be fitted to a linear line. This hints to power law dependencies.

We first consider  $\frac{\rho_R}{\rho_L} - 1$  as a function of the Péclet number. Figure 10a shows  $\frac{\rho_R}{\rho_L} - 1$  plotted against  $Pe$  for a few different  $\beta V_{\text{max}}$ ,  $\frac{x_R}{L_2}$  and  $\frac{x_L}{x_R} - 1$ . We clearly see a low and high Péclet number regime. In the low  $Pe$  regime, i.e.  $Pe \ll 1$ , the slopes of the fit lines are all equal to  $2 \pm 0.005$  and in the high  $Pe$  regime, i.e.  $Pe \gg 1$ , they are equal to  $-4 \pm 0.08$ . Thus, the dependency of  $\frac{\rho_R}{\rho_L} - 1$  on  $Pe$  is given by

$$\frac{\rho_R}{\rho_L} - 1 \sim \begin{cases} Pe^2 & \text{for } Pe \ll 1, \\ Pe^{-4} & \text{for } Pe \gg 1. \end{cases} \quad (4.7)$$

Notice that the slopes are independent of the other three system variables, i.e.  $\beta V_{\text{max}}$ ,  $\frac{x_R}{L_2}$  and  $\frac{x_L}{x_R} - 1$ , but that the Péclet number for which  $\frac{\rho_R}{\rho_L} - 1$  is largest does depend on these three variables. The low and high  $Pe$  regimes can be qualitatively explained by the activity of the particles. For  $Pe \ll 1$  the activity of the particles is almost negligible, hence the steady state distribution will resemble the passive steady state distribution for which  $\frac{\rho_R}{\rho_L} - 1 = 0$ . Increasing  $Pe$  increases the activity of the system, which in turn results in an increase of  $\frac{\rho_R}{\rho_L} - 1$ . However, when  $Pe \approx 1$ , further increasing  $Pe$  results in a decrease of  $\frac{\rho_R}{\rho_L} - 1$ . This decrease is caused by the fact that particles start to cross the ratchet with increasing ease. Therefore, when  $Pe \gg 1$ , particles can almost ignore the presence of the ratchet potential and thus,  $\rho_R \approx \rho_L$ .

Next, we consider  $\frac{\rho_R}{\rho_L} - 1$  as a function of the potential height. Figure 10b shows  $\frac{\rho_R}{\rho_L} - 1$  plotted against  $\beta V_{\text{max}}$  for a few different  $Pe$ ,  $\frac{x_R}{L_2}$  and  $\frac{x_L}{x_R} - 1$ . We see that  $\frac{\rho_R}{\rho_L} - 1 \downarrow 0$  for  $\beta V_{\text{max}} \downarrow 0$ , as is to be expected. After all, when  $\beta V_{\text{max}} \downarrow 0$ , the forces due to the ratchet potential become negligible small and consequently  $\frac{\rho_R}{\rho_L} - 1 \downarrow 0$ . For  $\beta V_{\text{max}} \lesssim 3$  the datasets can all be fitted to a line with slope equal to  $3 \pm 0.1$ . Thus,

$$\frac{\rho_R}{\rho_L} - 1 \sim (\beta V_{\text{max}})^3 \quad \text{for } \beta V_{\text{max}} \lesssim 3. \quad (4.8)$$

Notice that for high ratchet potentials, i.e.  $\beta V_{\text{max}} \gtrsim 3$ , the green data points deflect upwards from the corresponding fit line, while the other three datasets deflect down. Unfortunately, we could not discover the dependency of  $\frac{\rho_R}{\rho_L} - 1$  on  $\beta V_{\text{max}}$  in the high potential regime.

The third dependency we examine is  $\frac{\rho_R}{\rho_L} - 1$  as a function of the asymmetry of the ratchet potential. Figure 10c shows  $\frac{\rho_R}{\rho_L} - 1$  plotted against  $\frac{x_L}{x_R} - 1$  for a few different  $Pe$ ,  $\beta V_{\max}$  and  $\frac{x_R}{L_2}$ . To obtain the data we fix  $\frac{x_R}{L_2}$  and vary  $\frac{x_L}{L_2}$ . We see that the density difference increases for increasing asymmetry. This is to be expected, as  $\frac{\rho_R}{\rho_L} - 1 = 0$  for a symmetric, i.e.  $\frac{x_L}{x_R} - 1 = 0$ , ratchet and increasing the asymmetry increases the ease with which the particles cross the ratchet from the left. For  $\frac{x_L}{x_R} - 1 \ll 1$  the datasets can all be fitted to a line with slope equal to  $1 \pm 0.05$ . Thus,

$$\frac{\rho_R}{\rho_L} - 1 \sim \left( \frac{x_L}{x_R} - 1 \right) \quad \text{for } \frac{x_L}{x_R} - 1 \ll 1. \quad (4.9)$$

Lastly, we consider  $\frac{\rho_R}{\rho_L} - 1$  as a function of the ratchet size. Figure 10d shows  $\frac{\rho_R}{\rho_L} - 1$  plotted against  $\frac{x_R}{L_2}$  for a few different  $Pe$ ,  $\beta V_{\max}$  and  $\frac{x_L}{x_R} - 1$ . Naively we would expect  $\frac{\rho_R}{\rho_L} - 1$  to increase with increasing  $\frac{x_R}{L_2}$ , as we expect it to be more difficult for a particle to cross a ratchet the longer the ratchet gets. However, we see that this is not always the case, as  $\frac{x_L}{x_R} - 1$  decreases for  $\frac{x_R}{L_2} \gtrsim 1$ . This can be explained by the fact that the force due to the ratchet potential becomes almost negligible small, when  $\beta V_{\max}$  is fixed and  $\frac{x_R}{L_2} \rightarrow \infty$ . And even though this very small force acts over many lattice sites, the translational preference due to the orientation of the particles is far greater than the influence of the ratchet force. For  $\frac{x_R}{L_2} \gg 1$  the fit lines of figure 10d all have a slope of  $-2 \pm 0.05$ , thus our fourth and last dependency of  $\frac{\rho_R}{\rho_L} - 1$  is given by

$$\frac{\rho_R}{\rho_L} - 1 \sim \left( \frac{x_R}{L_2} \right)^{-2} \quad \text{for } \frac{x_R}{L_2} \gg 1. \quad (4.10)$$

For  $\frac{x_R}{L_2} \ll 1$  figure 10d also appears to pass into a power law dependency. Unfortunately, it is difficult to obtain data to examine this limit. The reason for this finds its origin in the earlier defined restrictions of our model, i.e.  $i_R, i_L \geq 40$  and  $\lambda \in [8a, \frac{L-x_R-x_L}{20}]$ . The first restriction implies that  $x_R$  should at least be equal to  $40a$ . Hence, since we cannot take  $x_R \ll 1$ , we need to take  $L_2 \gg 1$  to achieve  $\frac{x_R}{L_2} \ll 1$ . This, on its own, is easily accomplished. However, from Eq.(3.36) follows that  $\lambda \gg 1$ , when  $L_2 \gg 1$  and  $Pe$  is fixed. Thus, to meet the restriction  $\lambda < \frac{L-x_R-x_L}{20}$  the system size  $L$  should become even bigger than  $\lambda$ . In this lies the actual problem: increasing  $L$  also increases  $N$ , which results in an enormous matrix  $M^{\text{rat}}$  and this in turn results in extremely long calculation times for finding the steady state distribution. For this reason we also do not have data for  $\frac{x_R}{L_2} > 100$ ,  $\frac{x_L}{x_R} - 1 < 0.01$ ,  $\frac{x_L}{x_R} - 1 > 6$  and  $Pe > 50$ . These situations, all in their own way, demand a system with  $N \gg 4000$ , for which calculating the steady state distribution simply takes too long using *Mathematica*.

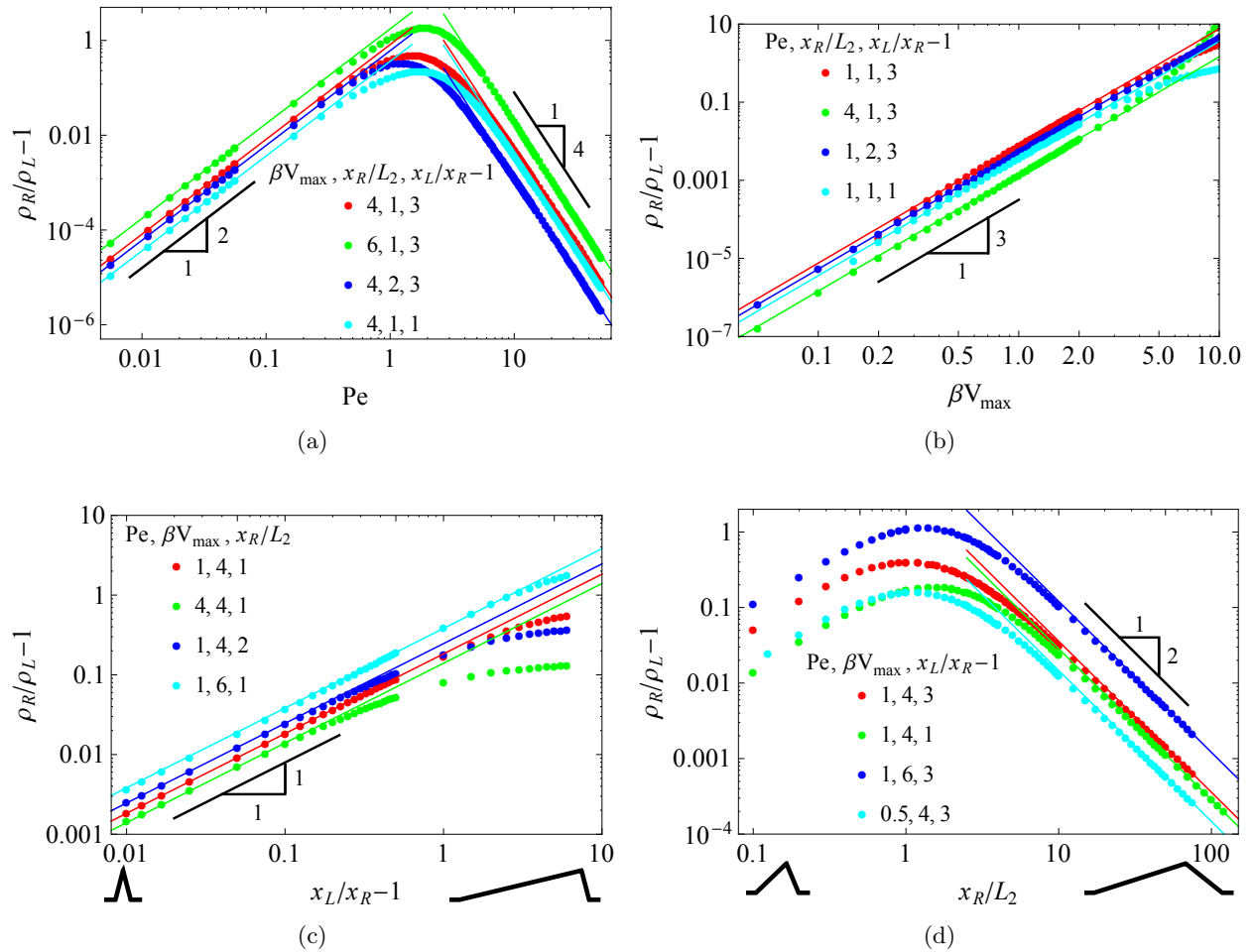


Figure 10: The bulk density difference  $\frac{\rho_R}{\rho_L} - 1$  plotted against (a) the Péclet number  $Pe$ , (b) the height of the ratchet potential  $\beta V_{\max}$ , (c) the length of the right side of the ratchet potential  $\frac{x_L}{x_R} - 1$  and (d) the asymmetry of the ratchet potential  $\frac{x_L}{x_R} - 1$ , all with logarithmic axes. The lines represent fit lines of the function  $y = ax^b$ . The small figures underneath the horizontal axes of (c) and (d) represent the shapes of the ratchet potential.



## 5 Conclusion, Discussion and Outlook

### 5.1 Conclusion

This thesis aims to develop a discrete model for an ideal active lattice gas to find a generalisation of the Boltzmann distribution for active systems. We specifically analyse the dependence on the particle activity of the particle accumulation at hard wall boundaries and the behaviour of active systems with an external ratchet potential. In chapter 2 we develop a lattice model using one parameter, i.e.  $\gamma$ , to characterise the activity of the system. The model considers the time evolution of a state to be described by a rotation step, in which a particle's orientation is maintained or changed with a probability dependent on  $\gamma$ , followed by a translation step, in which a particle translates along its orientation. However, we see that this one-parameter model is too heavily simplified and produces steady states without a length scale in the particle accumulation at the boundaries. Thus, in chapter 3 we adjust the translation step of the model by introducing a second parameter, i.e.  $\alpha$ , which serves as a measure for the probability of a particle to translate along the direction of its orientation. The steady state distributions produced by this two-parameter model are in good agreement with the continuum distributions, i.e. Eq.(3.45)-(3.46) and Eq.(3.49)-(3.50), derived from the Fokker-Planck equation, when we consider the continuum limit of our model, i.e.  $\alpha, \gamma \downarrow 0$ . We find that the particle accumulation at a hard wall boundary exponentially decays with a universal decay length  $\lambda$  given by

$$\lambda = \frac{L_2}{\sqrt{1 + \text{Pe}^2}}, \quad (5.1)$$

where  $L_2$  is the translational diffusion length scale and  $\text{Pe}$  is the Péclet number. Moreover, the density and polarisation distributions of a system with a hard wall boundary at  $x = 0$  are given by

$$\rho(x) = \rho_{\text{bulk}} \left( 1 + \text{Pe}^2 e^{-x/\lambda} \right), \quad (5.2)$$

$$m(x) = -\rho_{\text{bulk}} \text{Pe} \sqrt{1 + \text{Pe}^2} e^{-x/\lambda}, \quad (5.3)$$

where  $\rho_{\text{bulk}}$  is the density of the bulk.

In chapter 4 we examine the behaviour of a system with an external ratchet potential by implementing the influence of the potential in the translation step of our two-parameter model. We find that the steady state of a system with an external ratchet potential divides itself in two subsystems with their own bulk density and argue that the bulk density belonging to the steepest side of the ratchet, the right side in our definition, is greater than the bulk density belonging to the more gentle left side. The bulk density difference  $\frac{\rho_R}{\rho_L} - 1$  depends on the activity of the particles, i.e. the Péclet number, and three variables that define the ratchet: the height  $\beta V_{\text{max}}$ , the length of the right side  $\frac{x_R}{L_2}$  and the asymmetry  $\frac{x_L}{x_R} - 1$ . We numerically find a low and high Péclet number regime in which the dependency of the bulk density difference on  $\text{Pe}$  is given by

$$\frac{\rho_R}{\rho_L} - 1 \sim \begin{cases} \text{Pe}^2 & \text{for } \text{Pe} \ll 1, \\ \text{Pe}^{-4} & \text{for } \text{Pe} \gg 1. \end{cases} \quad (5.4)$$

Furthermore, we find that for flat and almost symmetric ratchet potentials, i.e. ratchets with a height  $\beta V_{\text{max}} \lesssim 3$ , length  $\frac{x_R}{L_2} \gg 1$  and asymmetry  $\frac{x_L}{x_R} - 1 \ll 1$ , the bulk density difference is given by

$$\frac{\rho_R}{\rho_L} - 1 \sim (\beta V_{\text{max}})^3 \left( \frac{x_R}{L_2} \right)^{-2} \left( \frac{x_L}{x_R} - 1 \right). \quad (5.5)$$

### 5.2 Discussion

The discrete lattice model developed and used in this thesis is a simplistic, yet accurate model. In section 3.6 we see that the calculated steady state distributions for systems without an external potential are in good agreement with the derived continuum distributions. Unfortunately, we have no continuum validation for the results obtained with an external ratchet potential. However, the observed behaviour of the bulk density difference is not unexpected, as is explained in section 4.3, and, in private conversation with J. Rodenburg, we find that numerical solutions of the differential equations provide similar results.

During our research we encountered a couple of limitations of our lattice model. The most obvious limitation considers the number of lattice sites  $N$ . Evidently, increasing  $N$  increases the calculation time. Calculations of systems with  $N$  up to the order of  $10^3$  typically take up to an hour per state, which is acceptable, but when  $N$  is of the order  $10^4$  or higher calculations using *Mathematica* typically take a day per state, which is simply too long. This, of course, is no surprise, since *Mathematica* was not made with the aim to solve large matrix equations. For future research it could be beneficial to invest in software specifically designed for solving large matrix equations, such that larger systems can be investigated.

Other limitations of our model consider extrema, such as small decay lengths, high Péclet numbers and very large, small, antisymmetric or almost symmetric ratchets. All these limitations directly or indirectly originate from the restriction on the number of lattice sites. The total length of the ratchet, for example, is directly restricted to the size of the system, while the minimum decay length is restricted to a couple of lattice constants, which in turn depends on  $N$ . For discrete models it is important to have a fine discretisation. The lattice constant  $a$  should be small enough such that examined phenomena, e.g. the decay of the accumulation or a ratchet potential, take place across a considerable number of lattice sites and for a system with size  $L = (N - 1)a$  a small lattice constant is accomplished when  $N$  is large. When using continuum models, one does not have to take this into account and arbitrary small decay lengths, large Péclet numbers and small ratchets can be easily studied. In future research continuum models can be used to examine these limits and check if our derived dependencies of the bulk density difference in systems with external ratchet potentials still holds.

### 5.3 Outlook

The discussion already provided a couple of recommendations for future research considering different software of continuum models. However, there are plenty more possibilities for future research using our discrete lattice model. For example, we only briefly looked at flux and flux rotation and left a lot to be examined. Another example that we only briefly discussed is two-dimensional systems. We mentioned two-dimensional systems in chapter 2, but did not discuss the two-parameter model for two-dimensional systems. However, we did develop this model. One could further research flux rotations in two-dimensional systems, examine the influence of different confinement shapes, or add chiral obstacles to study self-induced flow. The downside of discrete two-dimensional lattice models is the rapidly growing matrix dimensions, and consequently calculation times, for larger systems. For example, a system of 20 by 20 sites already has a  $1600 \times 1600$  transition matrix. Therefore, to truly be able study two-dimensional systems one should consider using faster software or continuum models. Lastly, there is additional research possible on external ratchet potentials. One could for example examine the steady state of a system with two ratchets for which the two steepest sides face each other, study the cascading steady state distribution of a system with a row of ratchets, or consider ratchet potentials in two-dimensional systems or in systems with periodic boundary conditions.

## 6 Acknowledgement

I would first like to thank my supervisor Prof. René van Roij of the Institute for Theoretical Physics at Utrecht University. Prof. van Roij always made time for me in his busy schedule and his office door was often open for an unscheduled question. He provided guidance, but also consistently allowed this thesis to be my own work.

I would also like to thank Jeroen Rodenburg MSc. for his help and expertise on active systems. As well as Siddharth Paliwal MSc. for comparing notes on active systems with a ratchet potential.

Finally, I must express my gratitude to Wies Uijttewaal for proofreading this thesis. Thank you.

Author

Marjolein de Jager

## A Eigenvalues of the Transition Matrix

In this appendix we study the transition matrix and examine its eigenvalues. For generality we consider the transition matrix  $M$  of the two-parameter model described in section 3.1. However, the transition matrix  $M'$  of the one-parameter model is equivalent to  $M$  when  $\alpha = 1$ .

The transition matrix describes the time evolution of a state  $|n(t)\rangle$ , i.e.

$$|n(t + \tau)\rangle = M|n(t)\rangle, \quad (\text{A.1})$$

and  $M$  is given by

$$M = TR = \begin{pmatrix} m_+ & m_+ & & & \\ m_- & 0 & m_+ & & \\ & \ddots & \ddots & \ddots & \\ & & m_- & 0 & m_+ \\ & & & m_- & m_- \end{pmatrix}, \quad m_{\pm} = \frac{1}{2} \begin{pmatrix} (1 \pm \alpha)(1 - \gamma) & (1 \pm \alpha)\gamma \\ (1 \mp \alpha)\gamma & (1 \mp \alpha)(1 - \gamma) \end{pmatrix}, \quad (\text{A.2})$$

where  $\alpha \in [0, 1]$  and  $\gamma \in [0, \frac{1}{2}]$  are the dimensionless model parameters.

A column  $i$  of  $M$  represents the probabilities of the particles in state  $i = (\vec{r}, \hat{e})$  transitioning to the other states of the system. The sum of a column must be equal to 1, such that there is no gain or loss of particles. Let us denote the eigenvalues of a system by  $\mu_i$ , with  $i = 1, \dots, 2N$ . For a system of  $N = 3$  sites the 6 eigenvalues of  $M$  are

$$\begin{aligned} &1, & \frac{\gamma}{2} + \frac{1}{2}\sqrt{(1-\gamma)^2 - \alpha^2(1-2\gamma)}, & -\frac{\gamma}{2} - \frac{1}{2}\sqrt{(1-\gamma)^2 - \alpha^2(1-2\gamma)}, \\ &1 - 2\gamma, & \frac{\gamma}{2} - \frac{1}{2}\sqrt{(1-\gamma)^2 - \alpha^2(1-2\gamma)}, & -\frac{\gamma}{2} + \frac{1}{2}\sqrt{(1-\gamma)^2 - \alpha^2(1-2\gamma)}, \end{aligned}$$

and for a system with  $N = 4$  sites the 8 eigenvalues are

$$\begin{aligned} &1, & 0, & \sqrt{\frac{1}{2} - \alpha^2(\frac{1}{2} - \gamma)}, & \sqrt{(1 - \alpha^2 - 2\gamma)(\frac{1}{2} - \gamma)}, \\ &1 - 2\gamma, & 0, & -\sqrt{\frac{1}{2} - \alpha^2(\frac{1}{2} - \gamma)}, & -\sqrt{(1 - \alpha^2 - 2\gamma)(\frac{1}{2} - \gamma)}. \end{aligned}$$

For larger systems the analytical solutions of the eigenvalues quickly become hideous and extremely hard or impossible to calculate. However, using numerical solutions we find that  $M$  has eigenvalues  $\mu_1 = 1$  and  $\mu_2 = 1 - 2\gamma$  for arbitrary  $\alpha$ ,  $\gamma$  and  $N$ . Notice that  $\mu_2 = 1$  when  $\gamma = 0$ . Furthermore, we find that all other eigenvalues  $\mu_i$  with  $i = 3, \dots, 2N$  exist in  $\pm$  pairs, i.e.  $\mu_j = -\mu_k$ , and have absolute values  $|\mu_i| < 1$  for arbitrary  $\alpha$ ,  $\gamma$  and  $N$ . Notice that some eigenvalues can be complex.

In section 2.2 we explained that the steady state  $|n_{ss}\rangle$  of a system can be found by solving  $|n_{ss}\rangle = M|n_{ss}\rangle$ , which corresponds to calculating the eigenvectors belonging to  $\mu_i = 1$ . Thus, we find that a system with arbitrary  $N$  has one unique steady state distribution when  $\gamma \neq 0$  and two in the extreme case where  $\gamma = 0$ . Another method, which also reaches the conclusion that the steady states are found by finding the eigenvectors belonging to  $\mu_i = 1$ , uses the fact that  $\mu_i^t$  vanishes for  $t \rightarrow \infty$ , when  $|\mu_i| < 1$ . Hence, the only eigenvectors in  $|n(t)\rangle = M^{t/\tau}|n(0)\rangle$ , which do not vanish when  $t/\tau \rightarrow \infty$ , are the eigenvectors belonging to  $\mu_i = 1$ . Since a steady state is reached when  $t \rightarrow \infty$ , these eigenvectors must correspond to the steady states of the system.

## B Continuum Limit of Lattice Model with Ratchet Potential

In this appendix we derive the continuum limit for the lattice model with a ratchet potential described in section 4.1. The derivation closely follows the derivation of the continuum limit done in section 3.3 for the two-parameter model with no external potential.

We start by determining the  $\epsilon$  dependency of the force term  $\beta F_i$ , such that we know the behaviour in the continuum limit, i.e. the limit of  $\epsilon \downarrow 0$ . Using Eq.(4.4) and Eq.(4.5) we calculate the velocity

$$\frac{\langle \Delta x \rangle_{i,e}}{\tau} = e(1 - 2\gamma) \frac{\alpha a}{\tau} + \frac{\beta F_i a}{4\tau}.$$

Recall that the velocity should remain finite when  $\epsilon \downarrow 0$  and that  $a \sim \epsilon$  and  $\tau \sim \epsilon^2$ . We therefore find  $\beta F_i \sim \epsilon$  and define  $\tilde{F}_i = \frac{F_i}{\epsilon}$ . Next, we derive the equivalent of the Fokker-Planck equation starting from our matrices  $R$  and  $T^{\text{rat}}$ . The Fokker-Planck equation with an external potential  $V(x)$  is given by

$$\partial_t \psi_e(x, t) = [-v_0 e + \beta D_t \partial_x V(x)] \partial_x \psi_e(x, t) + D_t \partial_{xx} \psi_e(x, t) + \frac{D_r}{2} [\psi_{-e}(x, t) - \psi_e(x, t)]. \quad (\text{B.1})$$

The derivation for  $R$  is already done in section 3.3. For the derivation of  $T^{\text{rat}}$  we start by finding the equivalent of Eq.(3.18)

$$T_{(i_2, e_2 | i_1, e_1)}^{\text{rat}} = \delta_{e_2, e_1} \left[ \left( \frac{1}{2} (1 + \epsilon \tilde{\alpha} e) + \frac{\beta \tilde{F}_{i_1}}{4} \right) \delta_{i_2, i_1 + 1} + \left( \frac{1}{2} (1 - \epsilon \tilde{\alpha} e) - \frac{\beta \tilde{F}_{i_1}}{4} \right) \delta_{i_2, i_1 - 1} \right]. \quad (\text{B.2})$$

Then, using Eq.(3.20) we rewrite and restate Eq.(B.2) to find

$$T^{\text{rat}} = \mathbb{1} + \epsilon^2 T^{\text{rat} (2)} + \mathcal{O}(\epsilon^3), \quad T_{e_2, e_1}^{\text{rat} (2)} = \delta_{e_2, e_1} \left[ - \left( e \tilde{\alpha} + \frac{\beta \tilde{F}_{i_1}}{2} \right) \tilde{a} \partial_x + \frac{1}{2} \tilde{a}^2 \partial_{xx} \right]. \quad (\text{B.3})$$

Finally, we find the equivalent of the Fokker-Planck equation by taking the limit of  $\epsilon \downarrow 0$  of

$$\partial_t \psi_e(x, t) + \mathcal{O}(\epsilon^2) = \left( \frac{T^{\text{rat} (2)}}{\tilde{\tau}} + \frac{R^{(2)}}{\tilde{\tau}} \right) \psi_e(x, t) + \mathcal{O}(\epsilon^2). \quad (\text{B.4})$$

We find

$$\partial_t \psi_e(x, t) = - \lim_{\epsilon \downarrow 0} \left( \frac{e \tilde{\alpha} \tilde{a}}{\tilde{\tau}} + \frac{\beta \tilde{F}_i \tilde{a}}{2\tau} \right) \partial_x \psi_e(x, t) + \frac{1}{2} \lim_{\epsilon \downarrow 0} \left( \frac{\tilde{\alpha}^2}{\tilde{\tau}} \right) \partial_{xx} \psi_e(x, t) + \lim_{\epsilon \downarrow 0} \left( \frac{\tilde{\gamma}}{\tilde{\tau}} \right) [\psi_{-e}(x, t) - \psi_e(x, t)]. \quad (\text{B.5})$$

Comparing this to the Fokker-Planck equation of Eq.(B.1) we find, besides the already derived Eq.(3.28)-(3.30),  $D_t \partial_x V(x) = - \lim_{\epsilon \downarrow 0} \left( \frac{\tilde{F}_i \tilde{a}}{2\tau} \right)$ . Now, using Eq.(3.29) we find

$$\partial_x V(x) = - \lim_{\epsilon \downarrow 0} \left( \frac{\tilde{F}_i}{\tilde{a}} \right) = - \lim_{\epsilon \downarrow 0} \left( \frac{F_i}{a} \right). \quad (\text{B.6})$$

Thus, we find that  $F_i$  is equal to the force due to the potential times the lattice constant, which is precisely our definition of  $F_i$  introduced in section 4.1.

## References

- [1] A. Kaiser, A. Peshkov, A. Sokolov, B. ten Hagen, H. Löwen, and I. S. Aranson, “Transport powered by bacterial turbulence,” *Physical Review Letters*, vol. 112, 4 2014.
- [2] C. Dombrowski, L. Cisneros, S. Chatkaew, R. E. Goldstein, and J. O. Kessler, “Self-concentration and large-scale coherence in bacterial dynamics,” *Physical Review Letters*, vol. 93, 8 2004.
- [3] O. Sozinova, Y. Jiang, D. Kaiser, and M. Alber, “A three-dimensional model of myxobacterial aggregation by contact-mediated interactions,” *Proceedings of the National Academy of Sciences of the United States of America*, vol. 102, 8 2005.
- [4] N. Komin, U. Erdmann, and L. Schimansky-Geier, “Random walk theory applied to daphnia motion,” *Fluctuation and Noise Letters*, vol. 04, 3 2004.
- [5] K. Drescher, K. C. Leptos, I. Tuval, T. Ishikawa, T. J. Pedley, and R. E. Goldstein, “Dancing volvox: Hydrodynamic bound states of swimming algae,” *Physical Review Letters*, vol. 102, 4 2009.
- [6] P. M. Kareiva and N. Shigesada, “Analyzing insect movement as a correlated random walk,” *Oecologia*, vol. 56, 2 1983.
- [7] D. R. Rubenstein and K. A. Hobson, “From birds to butterflies: animal movement patterns and stable isotopes,” *TRENDS in Ecology and Evolution*, vol. 19, 5 2004.
- [8] D. Sumpter, J. Buhl, and D. Biro, “Information transfer in moving animal groups,” *Theory in Biosciences*, vol. 127, 8 2007.
- [9] A. Cavagna, A. Cimarelli, I. Giardina, G. Parisi, R. Santagati, F. Stefanini, and M. Viale, “Scale-free correlations in starling flocks,” *Proceedings of the National Academy of Sciences of the United States of America*, vol. 107, 6 2010.
- [10] W. F. Paxton, K. C. Kistler, C. C. Olmeda, A. Sen, S. K. S. Angelo, Y. Cao, T. E. Mallouk, P. E. Lamert, and V. H. Crespi, “Catalytic nanomotors: autonomous movement of striped nanorods,” *Journal of the American Chemical Society*, vol. 126, 10 2004.
- [11] I. Buttinoni, J. Bialke, F. Kümmel, H. Löwen, C. Bechinger, and T. Speck, “Dynamical clustering and phase separation in suspensions of self-propelled colloidal particles,” *Physical Review Letters*, vol. 110, 6 2013.
- [12] G. Volpe, I. Buttinoni, D. Volgt, H. J. Kümmerer, and C. Bechinger, “Microswimmers in patterned environments,” *Soft Matter*, vol. 19, 8 2011.
- [13] Y. Fily, A. Baskaran, and M. F. Hagan, “Dynamics of self-propelled particles under strong confinement,” *Soft Matter*, vol. 10, 5 2014.
- [14] J. Tailleur and M. E. Cates, “Sedimentation, trapping, and rectification of dilute bacteria,” *Europhysics Letters*, vol. 86, 6 2009.
- [15] J. Palacci, C. Cottin-Bizonne, C. Ybert, and L. Bocquet, “Sedimentation and effective temperature of active colloidal suspensions,” *Physical Review Letters*, vol. 105, 8 2010.
- [16] L. Angelani, R. D. Leonardo, and G. Ruocco, “Self-starting micromotors in a bacterial bath,” *Physical Review Letter*, vol. 102, 1 2009.
- [17] P. K. Ghosh, V. R. Misko, F. Marchesoni, and F. Nori, “Self-propelled janus particles in a ratchet: Numerical simulations,” *Physical Review Letters*, vol. 110, 6 2013.
- [18] R. Ni, M. A. C. Stuart, and P. G. Bolhuis, “Tunable long range forces mediated by self-propelled colloidal hard spheres,” *Physical Review Letters*, vol. 114, 1 2015.

- 
- [19] R. Brown, "A brief account of microscopical observations made in the months of june, july and august 1827, on the particles contained in the pollen of plants; and on the general existence of active molecules in organic and inorganic bodies," *The Philosophical Magazine*, vol. 4, 1828.
- [20] P. Romanczuk, M. Bär, W. Ebeling, B. Lindner, and L. Schimansky-Geier, "Active brownian particles," *The European Physical Journal*, vol. 202, 3 2012.
- [21] C. Wiener, "Erklärung des atomistischen wesens des tropfbar flüssigen körperzustandes und bestätigung desselben durch die sogenannten molekularbewegungen," *Annalen der Physik*, vol. 17, 1905.
- [22] A. Einstein, "Investigation on the theory of the brownian movement," *Annalen der Physik*, vol. 17, 1905.
- [23] P. Langevin, "Sur la théorie du mouvement brownien," *Comptes Rendus Hebdomadaires des Séances de L'Academie des Sciences*, vol. 146, 1908.
- [24] M. von Smoluchowski, "Zur kinetischen theorie der brownischen molekularbewegung und der suspensionen," *Annalen der Physik*, vol. 326, 1906.
- [25] G. E. Uhlenbeck and L. S. Ornstein, "On the theory of the brownian motion," *Physical Review*, vol. 36, 9 1930.
- [26] D. Saintillan and M. J. Shelley, "Orientational order and instabilities in suspensions of self-locomoting rods," *Physical Review Letters*, vol. 99, 7 2007.
- [27] S. J. DeCamp, G. S. Redner, A. Baskaran, M. F. Hagan, and Z. Dogic, "Orientational order of motile defects in active nematics," *Nature Materials*, vol. 14, 8 2015.
- [28] M. Dijkstra, S. Paliwal, J. Rodenburg, and R. van Roij, "Chemical potential in active systems: Towards predicting phase equilibria from bulk equations of state using a swim potential." 9 2016.
- [29] W. Yan and J. F. Brady, "The force on a boundary in active matter," *Journal of Fluid Mechanics*, vol. 785, 11 2015.